

Article

Not peer-reviewed version

# A New 2D Cross Hyperchaotic Sine-Modulation-Logistic Map and Its Application in Bit-Level Image Encryption

[Mingxu Wang](#)\*, [Xianping Fu](#), Lin Teng, Xiaopeng Yan

Posted Date: 5 February 2024

doi: 10.20944/preprints202402.0205.v1

Keywords: 2D cross hyperchaotic map; Zig-zag transform; Cross coupled diffusion; Bit-level image encryption



Preprints.org is a free multidiscipline platform providing preprint service that is dedicated to making early versions of research outputs permanently available and citable. Preprints posted at Preprints.org appear in Web of Science, Crossref, Google Scholar, Scilit, Europe PMC.

Copyright: This is an open access article distributed under the Creative Commons Attribution License which permits unrestricted use, distribution, and reproduction in any medium, provided the original work is properly cited.

*Article*

# A New 2D Cross Hyperchaotic Sine-Modulation-Logistic Map and Its Application in Bit-Level Image Encryption

Mingxu Wang, Xianping Fu \*, Lin Teng \* and Xiaopeng Yan

School of Information Science and Technology, Dalian Maritime University, Dalian 116026, China

\* Correspondence: fxp@dmlu.edu.cn (X.F.); tenglin@dmlu.edu.cn (L.T.)

**Abstract:** Chaotic theory is commonly being researched for application in image encryption scheme (IES). In this paper, a novel two-dimensional cross hyperchaotic Sine-modulation-Logistic map (2D-CHSLM) based on the famous Sine and Logistic maps. The hyperchaotic behaviors of 2D-CHSLM is testified with the help of their bifurcation diagrams, trajectory plots, Lyapunov exponents, sample entropy, C0 complexity, permutation entropy and 0-1 test. A new bit-level IES with traditional encryption structure is proposed utilizing 2D-CHSLM. The 2D-CHSLM-IES performs a 2D-CHSLM-based bit-level confusion using zig-zag transform and a 2D-CHSLM-based cross coupled diffusion operations for generating a highly secure cipher-image. Then the simulations and security analyses are further carried out with the help of key space, key sensitivity, histogram, correlation, information entropy, differential attack, noise and data loss attacks, prove that the security of the proposed 2D-CHSLM-IES.

**Keywords:** 2D cross hyperchaotic map; zig-zag transform; cross coupled diffusion; bit-level image encryption

## 1. Introduction

Digital images play a big role in data communication through the networking or any technology, but their security is gradually arousing people's concern. Multiple image processing approaches were conceived, such as image encryption [1] and watermark [2]. Among them, image encryption scheme (IES) is essential to upholding solitude in image transmitting or safe storage, whether in medicine and military. Employing chaotic theories to enhance the security level of digital images demonstrates strong effectiveness. Chaotic map substantially impact cryptography [3] because it has characteristics of sensitivity to control parameters and initial conditions, pseudo-randomness, ergodicity, and unpredictability [4,5]. It is an effective and practical method to apply chaotic map to IES. Some newly advanced IESs based on chaotic maps using distinct technologies like Josephus traversal [6], deep learning [7], hash functions [8], DNA operation [9], and compression sensing [10] are proposed.

Chaotic maps (CM) are divided into one-dimensional (1D) depicted by difference formulas and high-dimensional (HD) defined by iterative differential formulas. The 1D chaotic map (1D-CM) has simple structure and is easy to implement in computer, which needs less time in the computation process. However, they are many flaws, such as the limited number of parameters and the uneven distribution of their generated state values. In contrast, the HD chaotic map (HD-CM) has more parameters, which can enlarge the range of chaotic behavior. Obviously, HD-CM has more complicated structure and will takes much time. Moreover, for IES, their security is greatly reliant on the performance of the CMs, so it is necessary to construct novel CMs with tremendous chaotic performance. Therefore, the construction of HD-CM is a feasible method to overcome the problems of 1D-CM. Recently, lots of advanced CMs have been designed. Wu et al [11] proposed an IES based on a two-dimensional Logistic map (2D-LM) with complicated basin structures and attractors. In [12], a novel IES based on the newly two-dimensional Sine Logistic modulation map (2D-SLMM) is proposed, which has the large chaotic range and better ergodicity. Sharma [13] designed a novel 2D-CM, which is derived from the idea of giving the two outputs of the 2D-LM to two separate 1D

Logistic maps. In [14], Zhu et al defined a 2D Logistic-modulated-sine-coupling-logistic chaotic map (2D-LSMCL), which is a modulation format of the Logistic and Sine maps. A 2D cross-mode hyperchaotic map based on the Logistic and Sine maps (2DCLSS) is presented by Teng et al [15] and then applied to a novel IES.

Since the first chaos-based IES was designed in 1989 [16], many chaos-based IESs have been proposed [17–20]. Based on Shannon's information theory, the basic structure of confusion-diffusion is generally adopted [21]. The confusion phase mainly includes two strategies: pixel-level and bit-level permutation. The pixel-level confusion will adjust the pixels' position while the pixels' value keeps invariable. However, the bit-level confusion has an advantage that the position and value of a pixel can be changed simultaneously [22]. Hence the bit-level confusion is regarded as more effective [23]. In the diffusion phase, the pixels' value would be modified. Some bit-level encryption algorithms are being proposed [24–27].

Motivated by the above analyses, this work introduced a novel bit-level IES by constructing a new 2D cross hyperchaotic Sine-modulation-Logistic map (2D-CHSLM) based on the famous Sine and Logistic maps (2D-CHSLM-IES). 2D-CHSLM-IES consists of three mainly parts, named the initial state calculation, 2D-CHSLM-based bit-level pixel permutation using zig-zag transform, and 2D-CHSLM-based cross coupled pixels diffusion strategy. Simulation tests demonstrate that 2D-CHSLM-IES is superior among the newly advanced IESs and has powerful robustness to the common types of the attacks. The rest of this paper is organized as follows: Section 2 describes and testifies 2D-CHSLM model. Section 3 outlines the related theories of 2D-CHSLM-IES. Section 4 details the newly proposed 2D-CHSLM-IES. The highly security of 2D-CHSLM-IES are analyzed in Section 5. Finally, the conclusions procured from the work are summarized in Section 6.

## 2. 2D-CHSLM model

This section introduces the proposed 2D-CHSLM and evaluates its hyperchaotic characteristics by comparing it with other existing 2D hyperchaotic maps (2D-HM).

### 2.1. Definition of 2D-CHSLM

For the common 1D-CMs with limited chaotic range, there is a possibility that the obtained sequences by them may perform weak randomness. It can be substantially avoided by constructing the HD-CM. A 2D-CHSLM is introduced through the cross format in the following. The Logistic map is widely studied traditional 1D-CM because of its complex chaotic behavior, which can be expressed by:

$$x_{n+1} = 4\mu x_n (1 - x_n) \quad (1)$$

where  $\mu$  represents the control parameter and Eq. (1) will enter in chaotic state when  $\mu \in [3.57, 4]$ . The Sine map is defined as:

$$x_{n+1} = 4\mu \sin(\pi x_n) \quad (2)$$

where the meanings of the parameters are consistent with Eq. (1). The bifurcation diagram is convenient tool to visualize the chaotic performance of Eq. (1) and Eq. (2). Figure 1 depicts the bifurcation diagram of Eq. (1) and Eq. (2) respectively (Here  $\mu = 0.1$ ). As can be seen in Figure 1, Eq. (1) and Eq. (2) have a small chaotic range, and there are many period windows. This section tries to designed a cross format to enhance their chaotic performance. Consequently, the mathematical formula of 2D-CHSLM is:

$$\begin{cases} x_{n+1} = F(G(y_n)) \\ y_{n+1} = G(F(\frac{x_n}{y_n})) \end{cases} \quad (3)$$

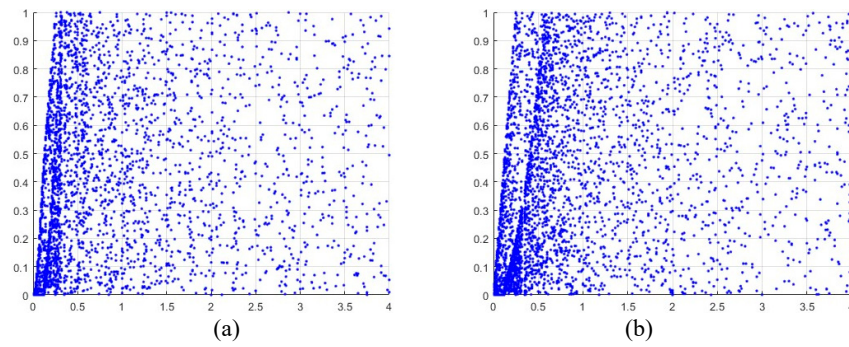
where  $F(\bullet)$  and  $G(\bullet)$  are the Eq. (2) and Eq. (2) respectively, and the control parameters is  $\mu$ . The variables  $x_{n+1}$  and  $y_{n+1}$  are obtained values by iterating over the initial variables  $x_n$  and  $y_n$ .

## 2.2. Performance evaluation of 2D-CHSLM

To analyze the nonlinearity, complexity, and unpredictability of 2D-CHSLM, several commonly metrics such as bifurcation and trajectory diagram, Lyapunov exponents, sample entropy, C0 complexity, permutation entropy, and 0-1 test are tested. Moreover, this section also compares the hyperchaotic performance of 2D-CHSLM with other advanced 2D-HMs.

### 2.2.1. Bifurcation diagram

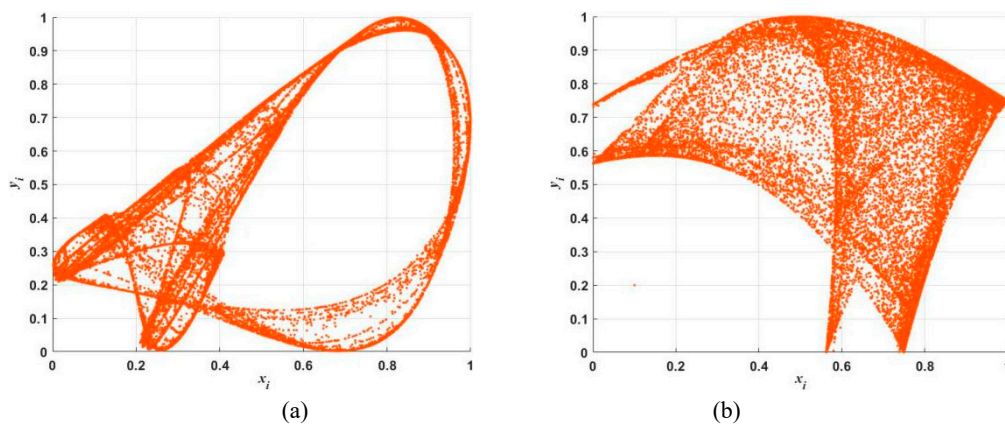
The bifurcation diagram (BD) reflects the advancement of time series as the parameters change. Therefore, BD can be used to measure the nonlinear characteristics of the CM [28–31]. Figure 2 depicts the BD of 2D-CHSLM with  $x_n$  and  $y_n$ , and the control parameter  $\mu$  within  $[0, 4]$ . As shown in Figure 2, 2D-CHSLM has a wide range, and has two iterative sequences that can be randomly distributed in whole space. It means that 2D-CHSLM has a large chaotic range.



**Figure 2.** BD of 2D-CHSLM: (a)  $x_n$  and (b)  $y_n$ .

### 2.2.2. Chaos trajectory

Trajectory of the chaotic attractor can directly reflect the nonlinearity and complexity of chaotic maps. For a periodic action, their trajectory is a locked curve. Chaos is bounded, and its trajectory is always limited to a certain range, which is called the chaotic attraction zone. Ideally, the trajectory of chaotic characteristics will not be locked or repeated, and it's usually occupying a fixed part of the phase space, which can mirror the randomness of the generated chaotic sequence. A large phase space means that the chaotic map can output good random values. When the initial values  $(x_0, y_0)$  of 2D-CHSLM are set to  $(0.1, 0.2)$ , the trajectory diagram is shown in Figure 3. Compared with other 2D-HMs, the trajectory diagram of 2D-CHSLM is more uniformly distributed and extensive. Hence 2D-CHSLM has more complex dynamic characteristics and wider chaotic range.



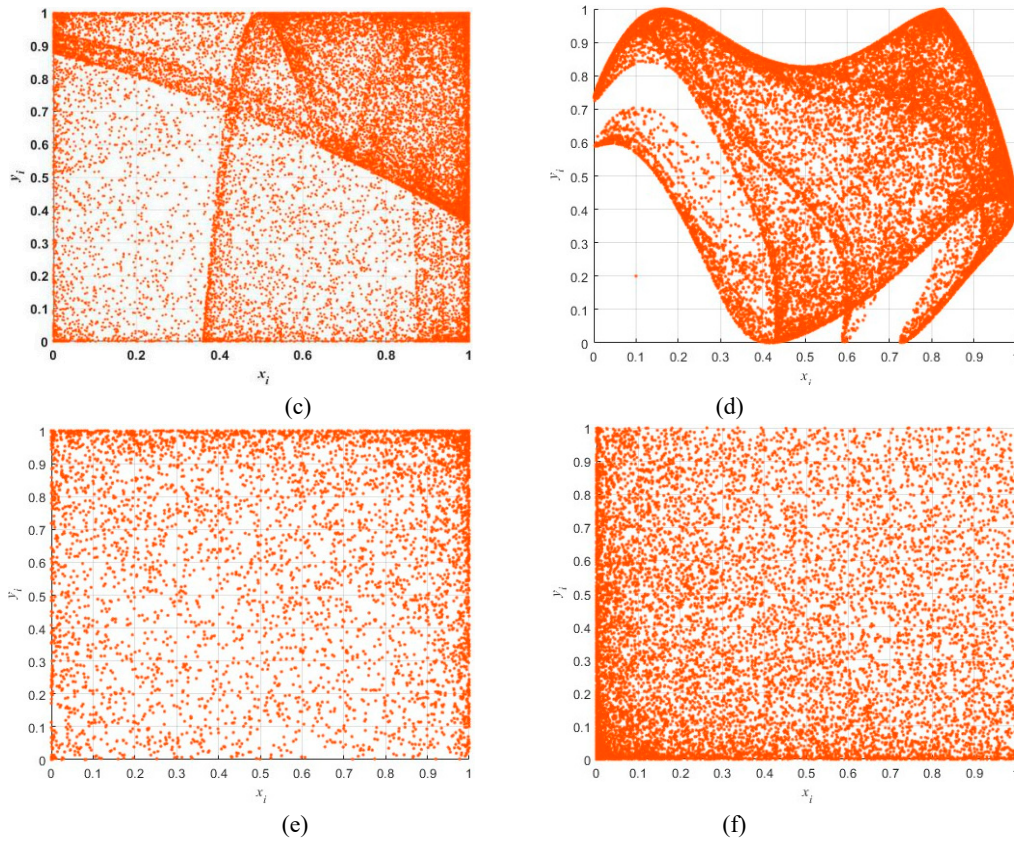


**Figure 3.** Trajectory plots. (a) 2D-LM, (b) 2D-SLMM, (c) 2D-LALM, (d) 2D-LSMCL, (e) 2D-CLSS, and (f) 2D-CHSLM.

### 2.2.3. Lyapunov exponent

For a CM, the Lyapunov exponent ( $LE$ ) is used to measure the proportion of convergence or divergence of the mean index for two adjacent orbits in phase space [32]. A positive  $LE$  value means that adjacent orbits are separated with each iteration, implying the emergence of chaotic state. If the CM has more than one positive  $LE$  value, implying the hyperchaotic characteristics. Specifically, a 2D-HM exhibits hyperchaotic characteristics when it has 2 positive  $LE$  values. This section firstly adopts the QR decomposition method [33] to analyze whether there is chaotic state in 2D-CHSLM. Its computed process is:

$$\begin{aligned}
 qr[J_M J_{M-1} \dots J_1] &= qr[J_M J_{M-1} \dots J_2 (J_1 Q_0)] \\
 &= qr[J_M J_{M-1} \dots J_3 (J_2 Q_1)] [R_1] \\
 &= qr[J_M J_{M-1} \dots J_i (J_{i-1} Q_{i-1})] [R_{i-1} \dots R_1] \\
 &= \dots \\
 &= Q_M [R_M \dots R_2 R_1] \\
 &= Q_M R
 \end{aligned} \tag{4}$$

where  $qr[\cdot]$  is the QR decomposition function and  $J$  represents the Jacobian matrix of the target 2D-HM. Subsequently, the  $LE$  of the chaotic map can be solved out via:

$$LE = \frac{1}{N} \sum_{i=1}^N \ln |R_i(v, v)|, \quad v = 1, 2, 3, \dots \tag{5}$$

Figure 4 depicts the  $LE$  value of 2D-CHSLM and the existing 2D chaotic maps (2D-CM) [11–15]. All 2D-CMs depicted from the initial state ( $x_0 = 0.1$ ,  $y_0 = 0.2$ ). Obviously, they exhibit chaotic characteristics. For 2D-CHSLM, their positive  $LE$  values are more than one, proving that there is hyperchaotic state. Specifically, the 2D-LM [11], 2D-SLMM [12], 2D-LALM [13], 2D-LSMCL [14], and 2D-CLSS [15] perform chaotic performance when the control parameter within (

$[1.11, 1.15] \cup [1.18, 1.19]$  and  $\beta = 3$ ),  $(0.87, 1)$ , and  $(0.3, 0.375) \cup (0.39, 0.965) \cup (0.21, 0.24) \cup (0.26, 0.36) \cup (0.39, 0.64) \cup (0.66, 1)$ , and  $((0, 0.078) \cup (0.095, 0.59) \cup (0.6, 0.66) \cup (0.66, 0.92) \cup (0.92, 2.09) \cup (2.09, 4])$ . 2D-CHSLM performs chaotic behaviors when  $[0.11, 0.31] \cup (0.33, 0.37) \cup [0.35, 2.03] \cup [2.07, 4]$ , which has larger chaotic range than other 2D-CMs. Moreover, 2D-SLMM, 2D-LALM, 2D-LSMCL, and 2D CLSS perform hyperchaotic behaviors when the control parameter within  $(0.905, 1)$ ,  $(0.415, 0.965) \cup (0.965, 1)$ ,  $(0.26, 0.36) \cup (0.39, 0.64) \cup (0.66, 1)$ , and  $(0.66, 0.92) \cup (0.92, 2.09) \cup (2.09, 4]$  respectively. 2D-CHSLM exhibits hyperchaotic behavior when  $[0.27, 0.31] \cup [0.45, 0.47] \cup [0.51, 2.03] \cup [2.07, 2.19] \cup [2.21, 4]$ . It can be concluded that 2D-CHSLM is significantly better than other advanced 2D-CMs and has wider application scenarios.

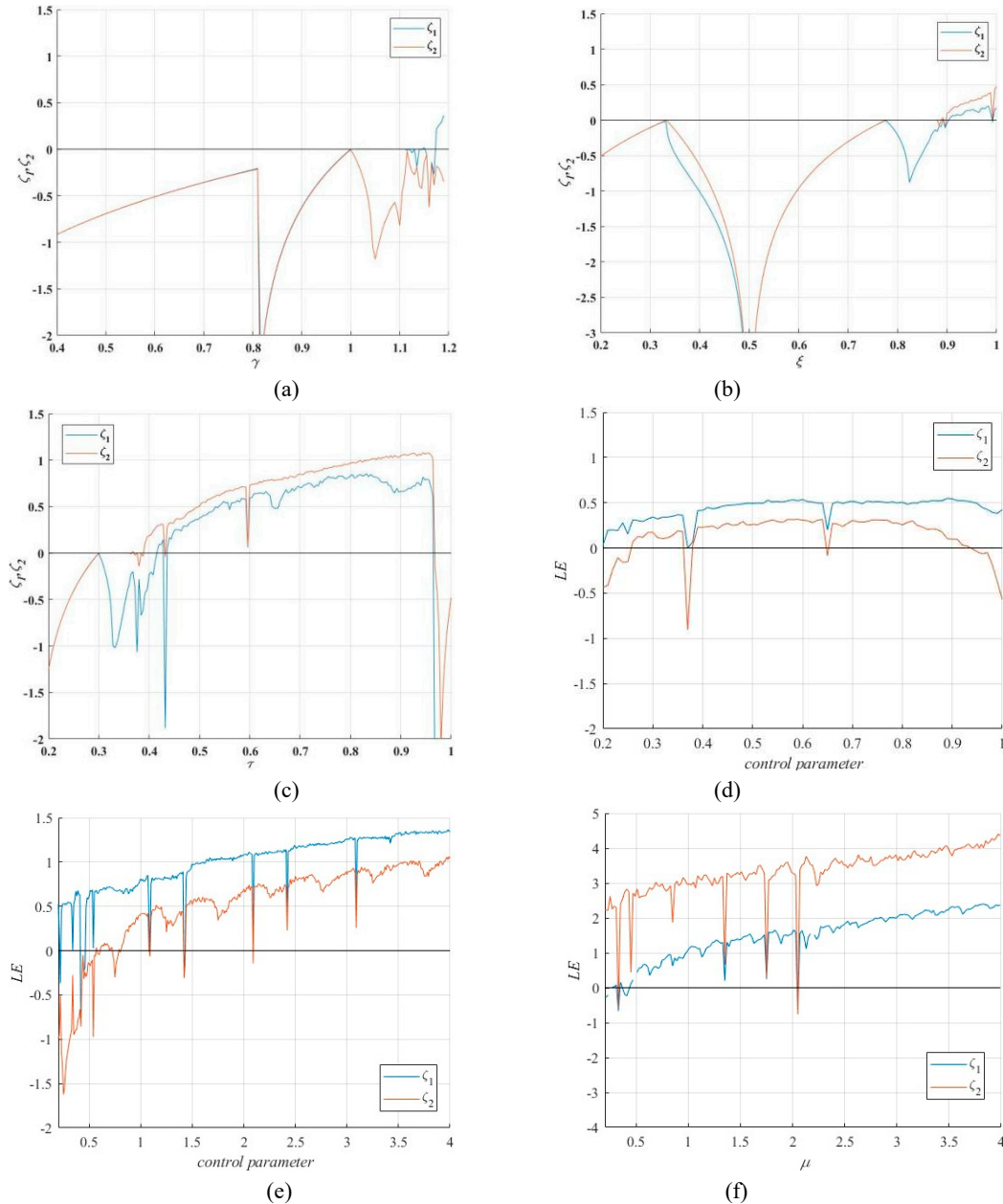


**Figure 4.** Variation of LE ( $\zeta_1$  and  $\zeta_2$ ) of (a) 2D-LM, (b) 2D-SLMM, (c) 2D-LALM, (d) 2D-LSMCL, (e) 2D-CLSS, and (f) 2D-CHSLM.

#### 2.2.4. Sample entropy

Sample entropy (SE) [34] is used to plot the oscillation patterns of time series, which is proportional to the intricacy of the series and can be calculated via:

$$SE(m, r, N) = -\log \frac{S}{P} \quad (6)$$

where  $m$ ,  $r$ , and  $N$  are the size of the template vector, the acceptance tolerance, and the length of the time series,  $S$  and  $P$  represent the Chebyshev distance between the template vector with  $i$  and  $j$ . Generally, a large SE value means that irregular sequences have high complexity. Figure 5 also compare the SE values of 2D-CHSLM with the existing 2D-CMs [11–15], all of which have huge volatilities and even have 0 values, except 2D-CHSLM which the average value is 1.7505, which is near 2. It indicated that 2D-CHSLM has better sequence complexity than other 2D-CMs.

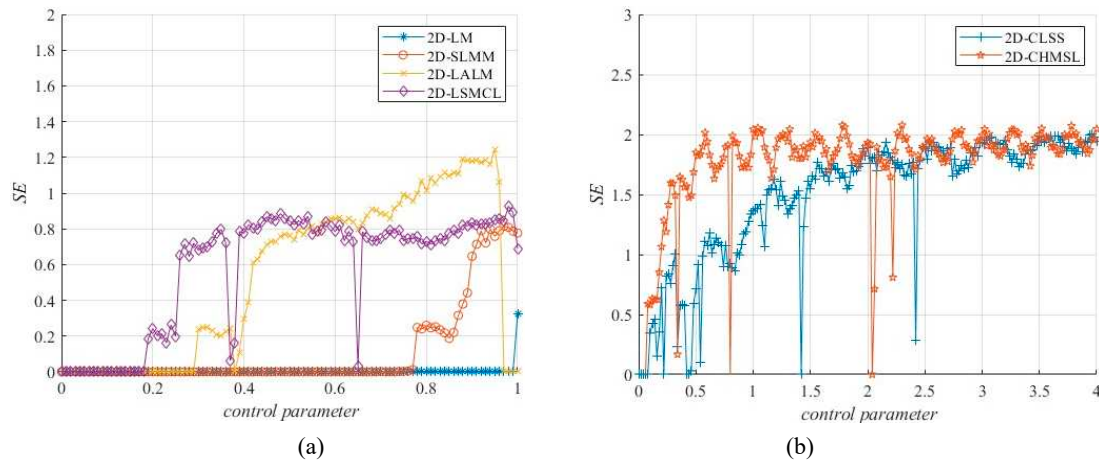


**Figure 5.** Variation of SE values of (a) 2D-LM, (b) 2D-SLMM, (c) 2D-LALM, (d) 2D-LSMCL, (e) 2D-CLSS, and (f) 2D-CHSLM.

### 2.2.5. C0 complexity

The system complexity is a significant method to analyze their dynamics. The complexity refers to the degree to which series is near random sequence. The bigger the complexity score is, the closer the series is to random series, and the higher the security of applied scheme will be. The complexity of CM can be divided into behavior and structure complexity respectively. Compare to the behavior complexity, the structural complexity, such as C0 method, performs more global statistical significance.

Figure 6 plots the C0 complexity results of 2D-CHSLM and compares with other 2D-CMs. As shown in Figure 6, all 2D-CMs except 2D-SLMM have biased C0s of 0, and the average C0 complexity value of 2D-CHSLM is 0.9374. It indicated that the complexity of 2D-CHSLM is relatively stable within the parameter range. Prove that the controllability and robustness of the chaotic sequence of 2D-CHSLM.

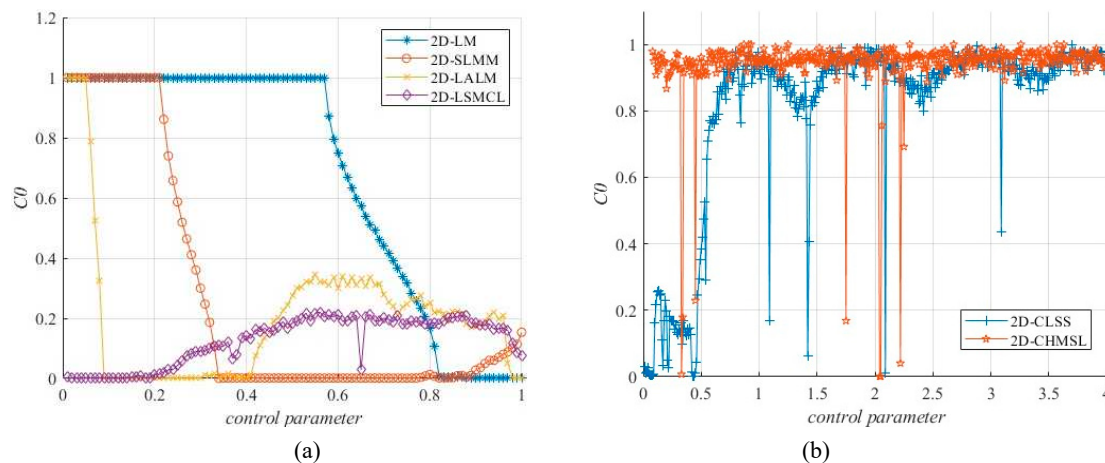


**Figure 6.** Variation of C0 values of (a) 2D-LM, (b) 2D-SLMM, (c) 2D-LALM, (d) 2D-LSMCL, (e) 2D-CLSS, and (f) 2D-CHSLM.

### 2.2.6. Permutation entropy

Permutation entropy (PE) [35] is another significant metric used to evaluate the complexity degree of time series. The complexity of chaotic map reflects the degree to which chaotic sequences approach pseudo-random sequences. The higher the complexity result is, the closer the sequence regards as a pseudo-random sequence, and the greater the security is. This section computes the complexity of 2D-CHSLM by their PE value.

Figure 7 plots a equivalence of the PE results of different 2D-CMs [11–15] under parameter swings, half of the 2D-CMs show the value of 0, while the rest illustrate great variation, the mean PE values of 2D-CHSLM is 0.9837, which testified 2D-CHSLM has superior and more steady sequence intricacy than other 2D-CMs.

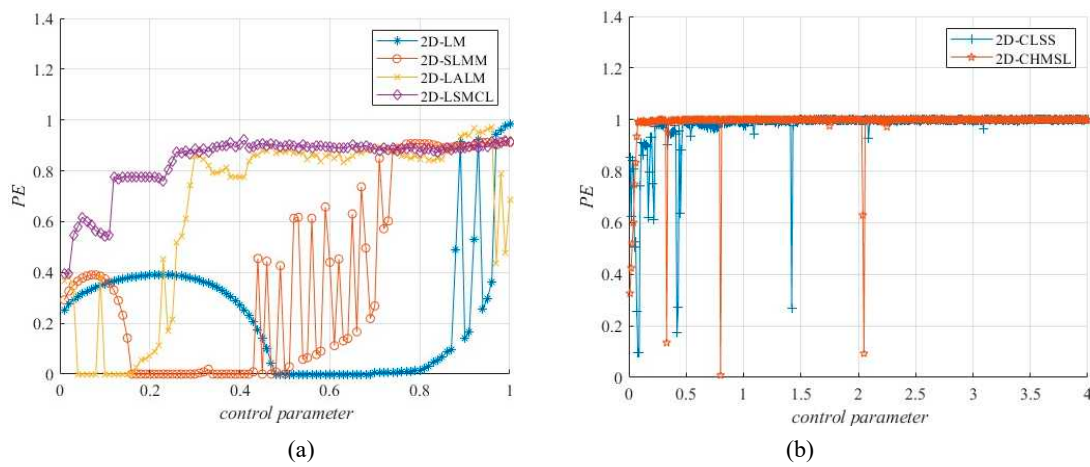


**Figure 7.** Variation of PE values of (a) 2D-LM, (b) 2D-SLMM, (c) 2D-LALM, (d) 2D-LSMCL, (e) 2D-CLSS, and (f) 2D-CHSLM.

### 2.2.70-1. Test

The 0-1 test is another important metric that evaluates the expansion rates of a nonlinear dynamic map's series. It can determine the frequency of non-ordinary fixed outcomes of any time series of a 2D-CM. Given a time series  $\varphi(j)$  for  $j = 1, 2, \dots, N$ , we execute the following steps,

$$p(n) = \sum_{j=1}^n \varphi(j) \cos(\theta(j)) \quad (7)$$

$$q(n) = \sum_{j=1}^n \varphi(j) \sin(\theta(j)) \quad (8)$$

$$\theta(j) = jc + \sum_{i=1}^j \varphi(i) \quad (9)$$

where  $c \in (0, 2\pi)$  is a casual constant,  $n = 1, 2, \dots, N$ ,  $j = 1, 2, \dots, n$ . Using  $p(n)$  and  $q(n)$ , the mean square displacement  $M(n)$  can be computed via:

$$M(n) = M_c(n) - (E(\phi))^2 ((1 - \cos nc) / (1 - \cos c)) \quad (10)$$

subject to,

$$M_c(n) = \lim_{N \rightarrow \infty} [(p(j+n) - p(j))^2 - (q(j+n) - q(j))^2] \quad (11)$$

$$E(\phi) = \lim_{N \rightarrow \infty} \frac{1}{N} \sum_{j=1}^N \phi(j) \quad (12)$$

if the trajectory of  $p(n)$  and  $q(n)$  performs the Brownian motion, then  $M(n)$  expands linearly with time. Otherwise, if the trajectories are bounded, then  $M(n)$  is bounded. The asymptotic growth proportion  $K_c$  of  $M(n)$  is:

$$K_c = \lim_{N \rightarrow \infty} \lg M(n) / \lg n \quad (13)$$

if  $K_c \approx 1$ , proved that the time series performs chaotic characteristics.

For comparative analyses, this section takes sample data  $N = 5000$ , and set the time series obtained by 2D-CHSLM as  $\phi(j)$ ,  $j = 1, 2, \dots, N$ . Based on the 0-1 test, the  $K_c$  of two time series  $p(n)$  and  $q(n)$  are respectively generated. The 2D-CLSS not exhibit chaotic performance when the control parameter near 2.09 (please see Figure 8a). When  $\mu = 3.99$ , the time series generated by 2D-CLSS performs chaotic behaviors (please see Figure 8b). As shown in Figure 8c, when  $\mu = 2.05$ , the time series generated by 2D-CHSLM doesn't perform chaotic behaviors. When  $\mu = 3.99$ ,  $K_c$  of two time series obtained by 2D-CHSLM are near 0.9971, which is close to 1, the time series enters in hyperchaotic state (please see Figure 8d).

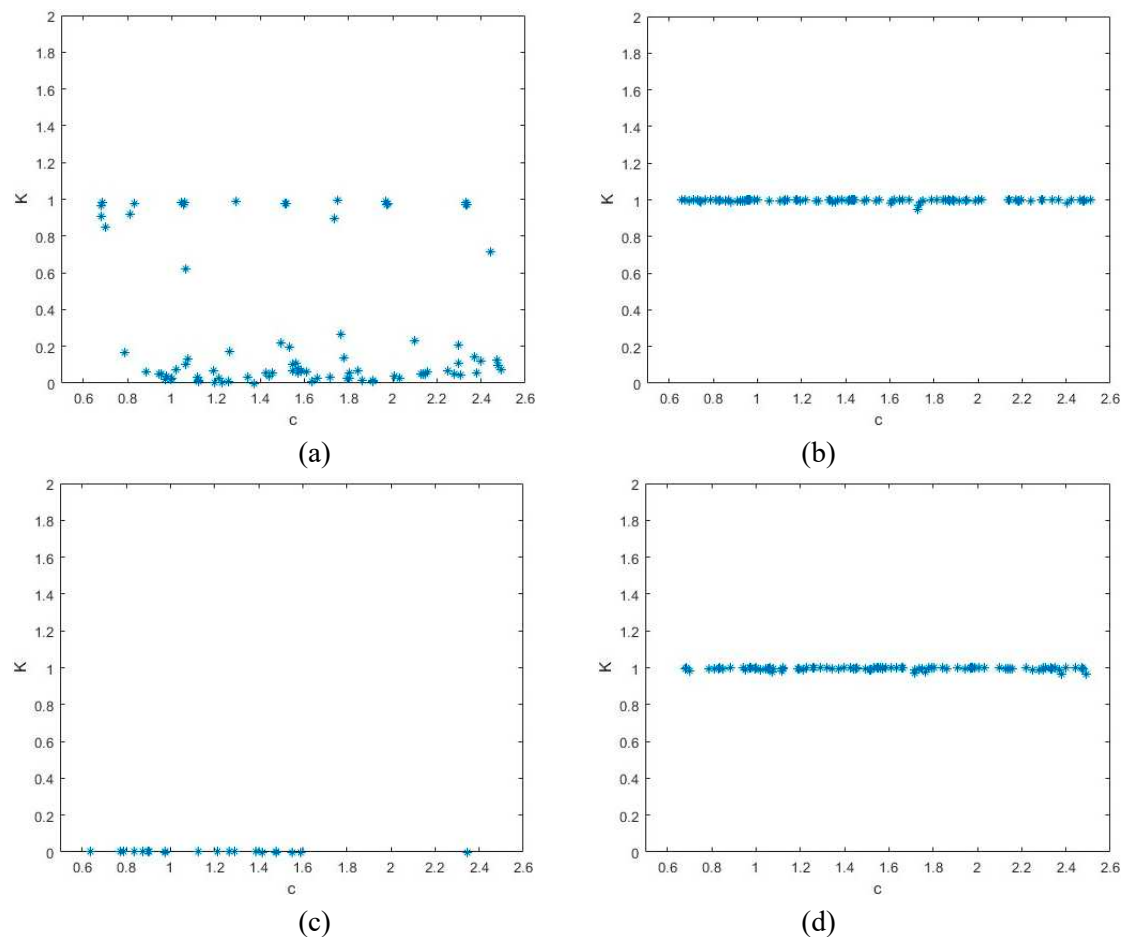


**Figure 8.** The asymptotic growth rate  $K_c$ : 2D CLSS at (a)  $\mu = 2.09$  and (b)  $\mu = 3.99$ , and 2D-CHSLM at (c)  $\mu = 2.05$  and (d)  $\mu = 3.99$ .

### 3. Related methods

### 3.1. Zig-zag transform

The elements in the matrix are sequentially traversed like a “Z” shape, and the traversed elements are sequentially stored in a one-dimensional array, and then transform into a two-dimensional matrix. This whole process is used to permutate the image matrix, named zig-zag transform. It can break the high correlation among image pixels to enhance the security level of IES [36].

Figure 9 depicted a traversed process of the zig-zag transform. For a permutation strategy based on zig-zag transform, the initial position plays a very important roles, different locations may generate different scrambled effects. For example, for a matrix (please see Figure 9a), if the initial position is (1, 1), that means traversing from the first pixel of the matrix, and Figure 9b depicted the matrix after zig-zag transform. This section performs zig-zag transform from the first and the last position of the matrix.

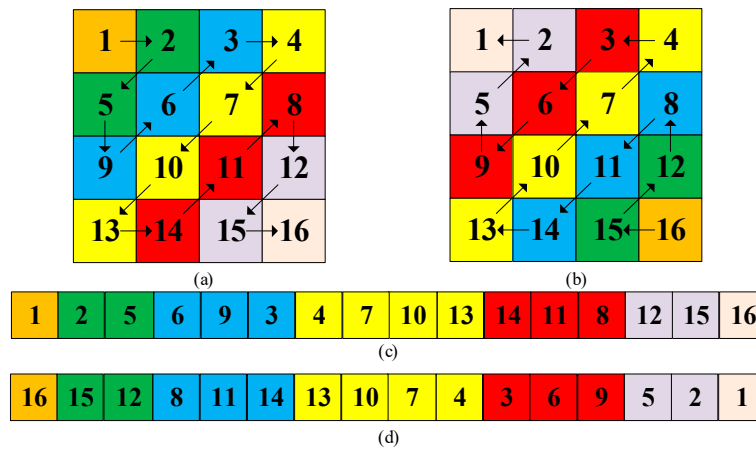


**Figure 9.** Zig-zag transform: a zig-zag path with starting pixel (a) (1,1) and (b) (4,4), the scanned result of (c) Figure 9(a) and (d) Figure 9(b).

### 3.2. Cross coupled pixels diffusion strategy

To enhance the diffusion effect, this section proposes a novel diffusion strategy, named cross coupled pixels diffusion (CCPD). In CCPD, the diffusion mechanism proceeds both in the row and column dimension. The diffused values of elements can be determined by their neighboring pixels' value. Specifically, the columns of the plain-image are dynamically divided into two groups. Then two groups perform CCPD process based on the row and column dimension. For the first group, the diffused values of all elements perform XOR operations via:

$$G'_1 = \begin{cases} G_1(i, j) \oplus CM_1(i, j) \oplus CM_1(i-1, j) \oplus CM_1(1, j) & \text{for } i=M \\ G_1(i, j) \oplus CM_1(i, j) \oplus CM_1(M, j) \oplus CM_1(i+1, j) & \text{for } i=1 \\ G_1(i, j) \oplus CM_1(i, j) \oplus CM_1(i-1, j) \oplus CM_1(i+1, j) & \text{for others} \end{cases} \quad (14)$$

where  $i-1$  and  $i+1$  represent the neighboring column pixel of  $i$ . Specially, when  $i=1$  and  $i=M$ , their neighboring columns are  $M$  and  $1$ , respectively.  $\oplus$  means the exclusive-OR operations.  $CM_1$  is the diffused matrix. Here  $M$  means the number of rows. For the second group, the diffused values of all elements perform XOR operations via:

$$G'_2 = \begin{cases} G_2(i, j) \oplus CM_2(i, j) \oplus CM_2(i, j-1) \oplus CM_2(i, 1) & \text{for } j=N \\ G_2(i, j) \oplus CM_2(i, j) \oplus CM_2(i, N) \oplus CM_2(i, j+1) & \text{for } j=1 \\ G_2(i, j) \oplus CM_2(i, j) \oplus CM_2(i, j-1) \oplus CM_2(i, j+1) & \text{for others} \end{cases} \quad (15)$$

where  $j-1$  and  $j+1$  represent the neighboring row pixel of  $j$ . Specially, when  $j=1$  and  $j=N$ , their neighboring columns are  $N$  and  $1$ , respectively.  $CM_2$  is the diffused matrix. Here  $N$  means the number of columns.

#### 4. The bit-level IES based on 2D-CHSLM

2D-CHSLM can generate highly complex hyperchaotic characteristics with a huge parameter variation. The generated sequence by 2D-CHSLM is uniform, covering the whole phase space. Hence 2D-CHSLM can be applied to IES to enhance its security. Based on 2D-CHSLM, this section further applies 2D-CHSLM to a novel IES, which consists of initial state calculation, 2D-CHSLM-based bit-level pixel permutation using zig-zag transform, and 2D-CHSLM-based coupled pixels diffusion strategy, named 2D-CHSLM-IES. Without loss of generality, the size of the plain-image ( $PI$ ) used in 2D-CHSLM-IES is  $M \times N$ .

##### 4.1. Initial state calculation

The key set of 2D-CHSLM-IES mainly consists of three parts, namely the hash value, the random binary array, and parameter key set respectively. The key structure of 2D-HLSM-CECP-IEA has depicted in Figure 11. For the hash value key set, due to the advantage of the hash function is that when making small adjustments to the input, the results are very sensitive and irreversible, making it highly effective against the plaintext attacks, which makes them very suitable for IES, hence the SHA-256 hash function is used to generate the hash value key set in 2D-CHSLM-IES, denoted as  $KS_{HV}$ . For the random binary array key set, this section randomly generates a binary array with a length of 208, denoted as  $KS_{BA} = \{bit_1, bit_2, \dots, bit_{208}\}$ . In addition, there are some variables in 2D-CHSLM-IES that serve as secret keys, namely  $KS_p = \{\mu, x_0, y_0, IT, OV\}$ . After initializing the key set  $KS = \{KS_{HV}, KS_{BS}, KS_p\}$ , the parameters are obtained and used in 2D-CHSLM to iteratively obtain the chaotic sequence. The detailed steps of  $KS$  are as follows:

Step 1: Input the plain-image  $PI$  into the SHA-256 hash function to generate a hexadecimal number  $HS$  with a length of 64, then convert  $HS$  to decimal and divide it into 8 parts as follows:

$$HS = \text{hash}(PI, 'SHA - 256') \quad (16)$$

$$KS_{HV} = \text{hex2dec}(HS(i:i+7)), i=1, 9, \dots, 57 \quad (17)$$

Among Eq. (16) and Eq. (17), the function  $\text{hash}(PI, 'SHA - 256')$  is used to compute the SHA-256 hash value of the input  $PI$ , whereas the function  $\text{hex2dec}(\bullet)$  is used to convert a hexadecimal string to their decimal format.  $HS(i:i+7)$  refers to the values of  $HS$  from the  $i$ -th to the  $i+7$ -th element.

Step 2: Initialize the random binary array  $KS_{BA}$ , then divide  $KS_{BA}$  into 4 sub-parts by converting into the floating-point numbers using the IEEE754 format via Eq. (18):

$$x = \frac{\sum_{i=1}^{52} b_i 2^{52-i}}{2^{52}} \quad (18)$$

Step 3: Initialize sub-keystream  $KS_p$  and use  $KS_{HV}$  and  $KS_{BA}$  to adjust the parameters of 2D-CHSLM-IES through Eq. (19):

$$\begin{cases} \mu' = \mu + ((\sum_{i=1}^{52} KS_{BA}[i] \times 2^{i-1}) / 2^{52}) \bmod (4 - \mu_0) \\ x'_0 = x_0 + ((\sum_{i=53}^{104} KS_{BA}[i] \times 2^{i-53}) / 2^{52}) \bmod (1 - x_0) \\ y'_0 = y_0 + ((\sum_{i=105}^{156} KS_{BA}[i] \times 2^{i-105}) / 2^{52}) \bmod (1 - y_0) \\ OV_1 = OV + \bmod(\text{floor}((\sum_{i=157}^{208} K[i] \times 2^{i-157}) / 2^{52}) \times 10^{15}, 256) \end{cases} \quad (19)$$

where  $\mu'$  is the control parameter of 2D-CHSLM.  $x'_0$  and  $y'_0$  are the initial parameter of 2D-CHSLM.  $OV_1$  means an offset value used in 2D-CHSLM-IES.

Step 4: Set  $\mu'$ ,  $x'_0$ , and  $y'_0$  as the parameters of 2D-CHSLM. Input them into of 2D-CHSLM for iteration  $IT + 4M \times N + hm_2 + hm_3$  times and exclude the first  $IT$  values to eliminate the transient effect. Since 2D-CHSLM is 2D, it outputs two iterative series referred to as  $CS_x$  and  $CS_y$ , then adjust  $CS_x$  and  $CS_y$  via:

$$\begin{cases} CS_x = \text{mod}(\text{floor}(CS_x(hm_2 + 1 : hm_2 + 4 \times M \times N)) \times 10^{15}, 256) \\ CS_y = \text{mod}(\text{floor}(CS_y(hm_3 + 1 : hm_3 + 4 \times M \times N)) \times 10^{15}, 256) \end{cases} \quad (20)$$

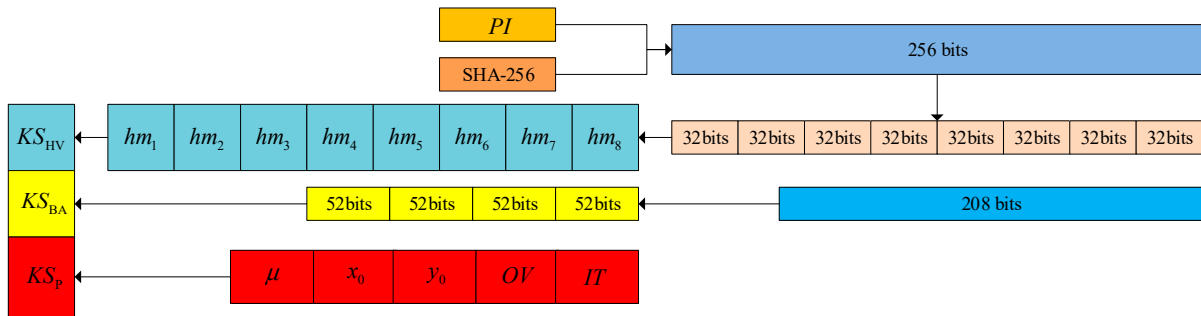


**Figure 11.** The structure of  $KS$ .

#### 4.2. 2D-CHSLM-based bit-level permutation using zig-zag transform

The permutation process comprises two parts: 2D-CHSLM-based bit plane grouping and sorting and 2D-CHSLM-based zig-zag transform. The specific steps are as follows:

Step 1: Read the plain-image  $PI$  and transform into 8 bit-planes, named  $PB_i (i = 1, 2, \dots, 8)$ . Initialize the key set  $KS_0$  based on Section 4.1.

Step 2: 2D-CHSLM-based bit plane grouping and sorting. Initialize a control sequence  $CS_{S\_PBP}$  for sorting  $PB_i (i = 1, 2, \dots, 8)$ . The index vector  $in\_CS_{S\_PBP}$  is obtained by sorting  $CS_{S\_PBP}$  in ascending order.  $CS_{S\_PBP}$  and  $in\_CS_{S\_PBP}$  are obtained as follows:

$$CS_{S\_PBP} = CS_x(hm_4 + 1 : hm_4 + 8) \quad (21)$$

$$(\sim, in\_CS_{S\_PBP}) = \text{sort}(CS_{S\_PBP}) \quad (22)$$

where  $\text{sort}(\bullet)$  is the sort function, which is used to sort the array and return the sorted array and index vector. To obtain only the index vector  $in\_CS_{S\_PBP}$ , this section can use the “ $\sim$ ” symbol to ignore the sorted array. Then divide  $PB_i (i = 1, 2, \dots, 8)$  into two groups  $FG$  and  $SG$  as follows:

$$FG = \{PB_{in\_CS_{S\_PBP}(1)}, PB_{in\_CS_{S\_PBP}(2)}, PB_{in\_CS_{S\_PBP}(3)}, PB_{in\_CS_{S\_PBP}(4)}\} \quad (23)$$

$$SG = \{PB_{in\_CS_{S\_PBP}(5)}, PB_{in\_CS_{S\_PBP}(6)}, PB_{in\_CS_{S\_PBP}(7)}, PB_{in\_CS_{S\_PBP}(8)}\} \quad (24)$$

Step 3: 2D-CHSLM-based zig-zag transform. Perform zig-zag transform on  $FG$  and  $SG$  respectively. For  $FG$ , scanning from the first element. For  $SG$ , scanning from the last element. The specific steps are shown in Section 3.1. The scanned  $FG$  and  $SG$  are saved as  $ZR_{FG}$  and  $ZR_{SG}$ . Then we sort  $ZR_{FG}$  and  $ZR_{SG}$  based on the index vector  $in\_CS_x$  and  $in\_CS_y$ .  $in\_CS_x$  and  $in\_CS_y$  are obtained as follows:

$$(\sim, in\_CS_x) = \text{sort}(CS_x) \quad (25)$$

$$(\sim, in\_CS_y) = \text{sort}(CS_y) \quad (26)$$

The sorted  $ZR_{FG}$  and  $ZR_{SG}$  are  $SR_{ZR_{FG}}$  and  $SR_{ZR_{SG}}$ . Lastly, divide  $SR_{ZR_{FG}}$  and  $SR_{ZR_{SG}}$  into 8 bit-planes, named  $PB'_i (i=1,2,\dots,8)$  and merge into a decimal permuted plain-image  $PI_{PI}$ .

#### 4.3. 2D-CHSLM-based coupled pixel diffusion

The diffusion process comprises two parts: 2D-CHSLM-based dynamical image blocking and 2D-CHSLM-based cross coupled pixels diffusion. The specific steps are as follows:

Step 1: 2D-CHSLM-based dynamical image blocking. Initialize a diffused control sequence  $DCS$  for blocking  $PI_{PI}$ . The index vector  $in\_DCS$  is obtained by sorting  $DCS$  in ascending order.  $DCS$  and  $in\_DCS$  are obtained as follows:

$$CS_x = CS_x(hm_5 + 1 : hm_5 + N) \quad (27)$$

$$(\sim, in\_DCS) = sort(DCS) \quad (28)$$

Then divide  $in\_DCS$  into two groups  $in\_DCS_1$  and  $in\_DCS_2$  based on  $OV_1$  and  $HM$  via:

$$\begin{cases} in\_DCS_1 = in\_DCS(1 : N / 2 - OV_1 - hm_6) \\ in\_DCS_2 = in\_DCS(N / 2 - OV_1 - hm_6 + 1 : N) \end{cases} \quad (29)$$

Step 2: 2D-CHSLM-based cross coupled pixels diffusion. Select two sub-sequences from  $CS_y$  as diffused value matrix, named  $DVS_1$  and  $DVS_2$ .  $DCS$  and  $in\_DCS$  are obtained as follows:

$$\begin{cases} DVS_1 = CS_y(hm_7 + 1 : hm_7 + M \times N) \\ DVS_2 = CS_y(hm_8 + M \times N + 1 : hm_8 + 2 \times M \times N) \end{cases} \quad (30)$$

On the one hand, select the columns from  $PI_{PI}$  and  $DVS_1$  based on  $in\_DCS_1$ , and perform diffused operations using Eq. (14) mentioned in Section 3.2. On the other hand, select the columns from  $PI_{PI}$  and  $DVS_2$  based on  $in\_DCS_2$ , and perform diffused operations using Eq. (15) mentioned in Section 3.2. Then saved the obtained diffused matrix as the cipher-image  $CI_{PI}$ .

After processing  $PI$  by Section 4, 2D-CHSLM-IES is finished. The inverse process of 2D-CHSLM-IES is named 2D-CHSLM-IDS. Obviously, it needs to reverse 2D-CHSLM-IES because the proposed 2D-CHSLM-IES is a symmetric cryptosystem. Figure 12 plotted the flowchart of 2D-CHSLM-IES.

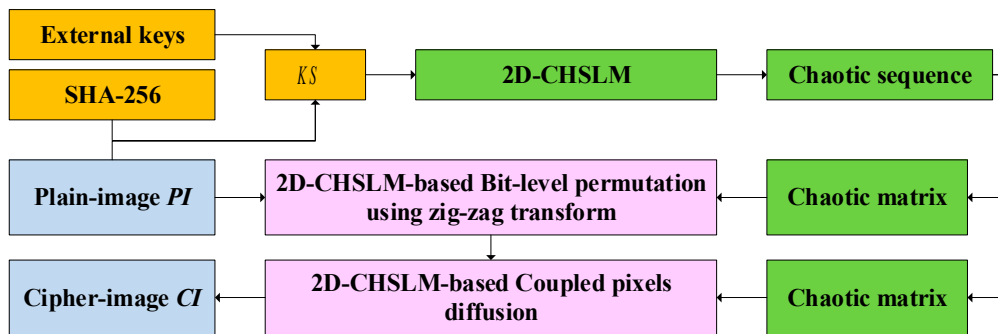


Figure 12. The flowchart of 2D-CHSLM-IES.

## 5. Experimental results and security analyses

To validate the robustness of 2D-CHSLM-IES, this section performs a comprehensive array of experiment and security analysis. The conducted analysis consists of key space analysis, key sensitivity analysis, histogram analysis, correlation coefficient analysis, information entropy analysis, differential attacks analysis, noise and data loss attacks analysis, is executed to assess the efficacy of 2D-CHSLM-IES. The plain-images drawn from the SIPI image databases (<https://sipi.usc.edu/database/database.php?volume=misc>). These analyses are performed utilizing the

MATLAB 2022a running on a compatible computer with Windows 10, 8 GB of RAM, and an Intel(R) CPU Core I5 2.80GHz.

### 5.1. Visual analysis

To verify the efficiency of the proposed 2D-CHSLM-IES, this section uses several plain-images of different size to stimulate the process. Setting the key stream of 2D-CHSLM-IES. As can be observed from Figure 13, the cipher-images obtained by 2D-CHSLM-IES totally hides the information of their corresponding plain-images, and the decrypted images obtained by 2D-CHSLM-IDS are the same as their original ones. It indicates that the proposed 2D-CHSLM-IES and 2D-CHSLM-IDS can perform the effective security operations of the digital plain-image.

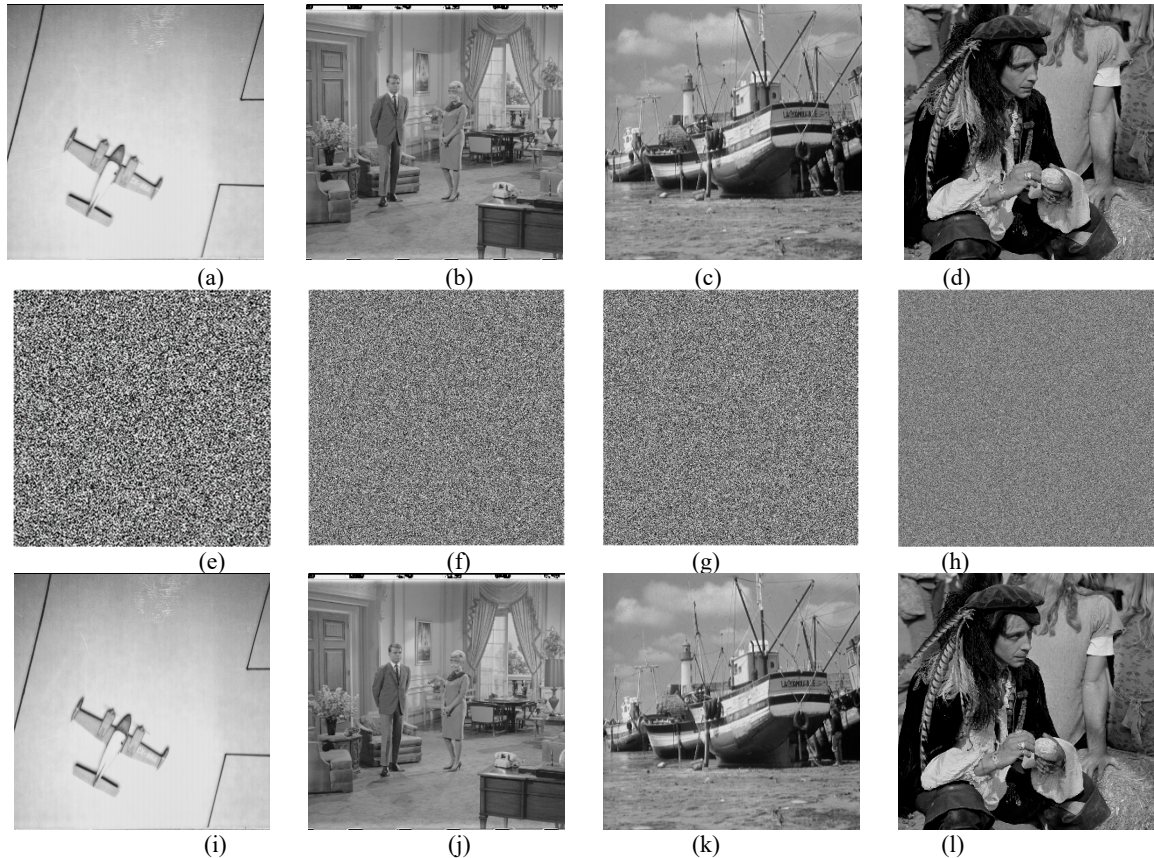


**Figure 13.** The plain, cipher and decrypted images of 2D-CHSLM-IES: the plain-image (a) 5.1.11, (b) 5.2.08, (c) boat.512, and (d) 5.3.01, the cipher-image of (e) Figure 13(a), (f) Figure 13(b), (g) Figure 13(c), and (h) Figure 13(d), and the decrypted image of (i) Figure 13(e), (j) Figure 13(f), (k) Figure 13(g), and (l) Figure 13(h).

### 5.2. Key space

A large key space is necessary to withstand the brute force attacks. To enhance the security of IES, the key space should larger than  $2^{100}$  [37]. Suppose the calculation accuracy of 2D-CHSLM-IES is around  $10^{15}$ , thereby the key space of independent keys is  $10^{15}$  respectively. In 2D-CHSLM-IES, it is  $KS_p = \{\mu, x_0, y_0, IT, OV\}$ . The key space of them can be accumulated as follows:

$$10^{15} \times 10^{15} \times 10^{15} \times 10^{15} \times 10^{15} = 10^{75} > 2^{225} \quad (31)$$

Moreover, SHA-256 is used in 2D-CHSLM-IES to initialize a non-independent hash key set  $KS_{HV}$ , and a 208-bits  $KS_{BA}$  is random initialize to be another part of key set. Both  $KS_{HV}$  and  $KS_{BA}$  are all used to adjust the original parameters of 2D-CHSLM-IES, and it can be considered that their

key space is  $2^{64} + 2^{208} = 2^{272}$ . whole key space of 2D-CHSLM-IES is larger than  $2^{497}$ , which is far larger than  $2^{100}$ . Hence 2D-CHSLM-IES can make the brute force attacks ineffective.

### 5.3. Key sensitivity

Key sensitivity indicates that even if there is a tiny modification in key set, IES cannot decode their cipher-image. A tremendous IES must have high key sensitivity. This section has checked the key sensitivity of 2D-CHSLM-IES. To create a novel key set, a tiny modification  $\Delta = 10^{-15}$  is respectively added to the original key set as follows:

$$KS_p = \{\mu_0, x_0, y_0, OV\}$$

$$KS_1 = \{\mu_0 + \Delta, x_0, y_0, OV\}$$

$$KS_2 = \{\mu_0, x_0 - \Delta, y_0, OV\}$$

$$KS_3 = \{\mu_0, x_0, y_0 + \Delta, OV\}$$

$$KS_4 = \{\mu_0, x_0, y_0, OV - \Delta\}$$

Figure 14 depicts the key sensitivity results using  $KS_0$  and  $KS_1$  on 2D-CHSLM-IES and 2D-CHSLM-IDS. Figure 14d is the pixel-to-pixel differential image of Figure 14b,c. It can be noted from Figure 4 the original image is successfully decoded only by matching key set. Prove that 2D-CHSLM-IES is completely sensitive to key set.

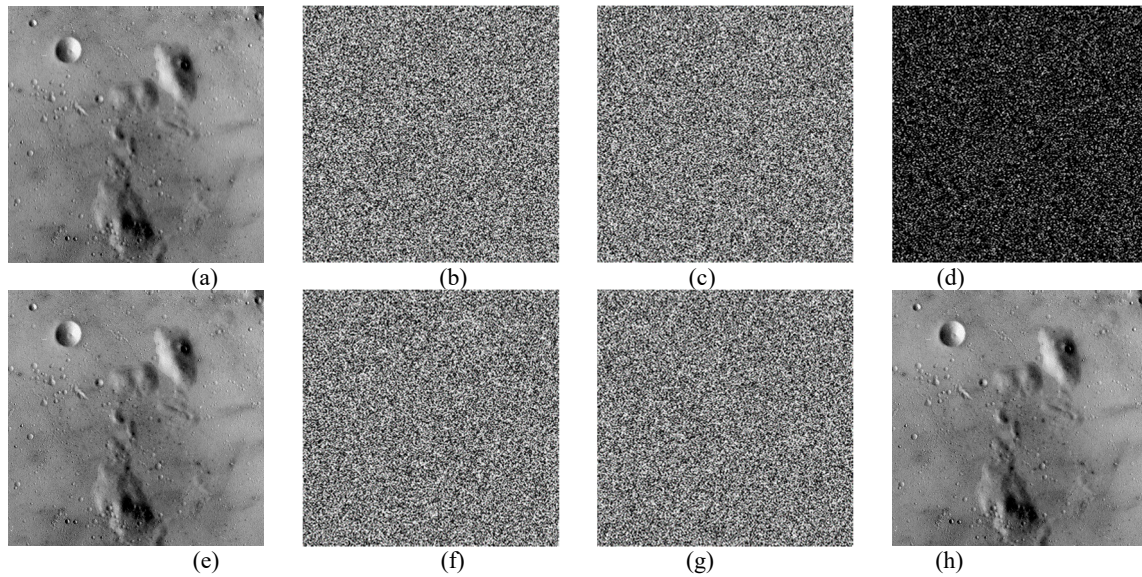


**Figure 14.** Key sensitivity result: (a) the plain image "5.1.09", the cipher-image of Figure 14(a) using (b)  $KS_0$  and (c)  $KS_1$ , (d) the differential image of Figs. 14(b) and 14(c), the decoded image of Figure 14(b) using (e)  $KS_0$  and (f)  $KS_1$ , the decoded image of Figure 14(c) using (g)  $KS_0$  and (h)  $KS_1$ .

### 5.4. Histogram

In IES breaking, the usual approach is to find the statistical characteristics of the cipher-image. Those properties can be analyzed by their histogram, which can give expression to the distribution pattern of their gray values. The flatter the histogram distribution is, the less the correlation between the image pixels' value and the number of pixels, and the more difficult to decode the plain-image information. The histogram tests of 2D-CHSLM-IES and 2D-CHSLM-IDS are shown in Figure 15. As can be observed in Figure 15, the histogram of the plain-image exhibits obvious statistical properties. After 2D-CHSLM-IES is performed, the histogram of the cipher-image is uniformly distributed. In Figure 15, the histogram of the decrypted image obtained by 2D-CHSLM-IDS is the same as their original image.

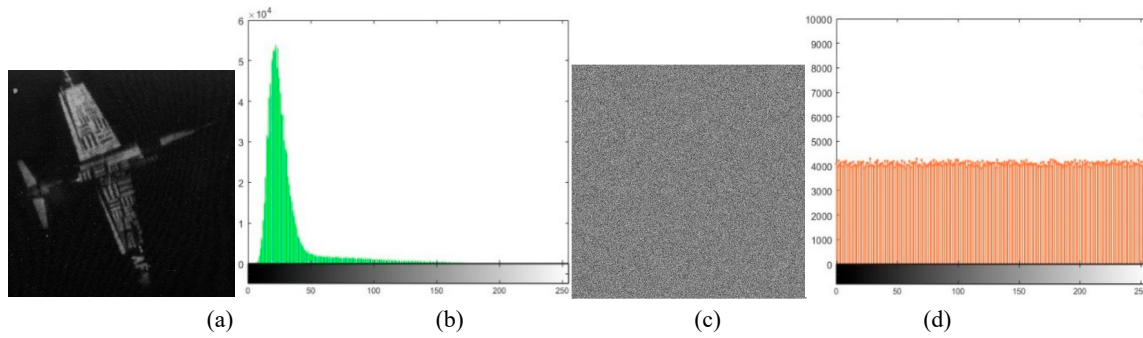


**Figure 15.** Histogram: (a) the plain-image 5.1.11 and the histogram of (b) Figure 14(a), (c) the cipher-image of 5.1.11 and the histogram of (d) Figure 15(c).

Moreover, this section further uses the chi-square ( $\chi^2$ ) test [38] to verify the uniform distribution of the histogram. For a grayscale image of size  $M \times N$ , supposed the pixel value distribution  $f$  of each pixel in the histogram is evenly distributed,  $h$  is the theoretical pixel value distribution, the computed value is  $M \times N / 256$ , and  $i$  is the brightness of the grayscale image, and follows the distribution of  $\chi^2$  with 255 degrees of freedom:

$$\chi^2 = \sum_{i=1}^n \frac{(f_i - h_i)^2}{h_i}. \quad (31)$$

When  $H = 0$ , it means the value passes the test. The calculation results tabulated in Table 1 illustrated the computed  $\chi^2$  test results of the cipher-images, which indicates that the gray distribution of the cipher-image is uniform.

**Table 1.**  $\chi^2$  test results.

Test image	Size	$\chi^2$	P-values	$H = 0$	Decision (H=0 or 1)
5.1.09	256×256	253.2188	0.1940	0	Accepted
5.1.10	256×256	230.9609	0.7099	0	Accepted
5.1.11	256×256	218.9922	0.6540	0	Accepted
5.1.12	256×256	240.5078	0.3791	0	Accepted
5.1.14	256×256	240.1172	0.1339	0	Accepted
5.2.08	512×512	269.8145	0.7031	0	Accepted
5.2.09	512×512	236.5098	0.2511	0	Accepted
5.2.10	512×512	276.7363	0.4475	0	Accepted
7.1.01	512×512	268.9434	0.5625	0	Accepted
7.1.02	512×512	315.0625	0.2259	0	Accepted
7.1.03	512×512	242.1719	0.0453	0	Accepted
7.1.04	512×512	235.498	0.9711	0	Accepted
7.1.05	512×512	292.6602	0.5090	0	Accepted
7.1.06	512×512	237.9414	0.2222	0	Accepted
7.1.07	512×512	311.0371	0.2414	0	Accepted
7.1.08	512×512	225.7656	0.2992	0	Accepted
7.1.09	512×512	302.6230	0.3242	0	Accepted

7.1.10	512×512	225.2598	0.2378	0	Accepted
boat.512	512×512	267.3926	0.1914	0	Accepted
gray21.512	512×512	266.9336	0.2579	0	Accepted
5.3.01	1024×1024	337.5430	0.0850	0	Accepted
5.3.02	1024×1024	316.2832	0.3871	0	Accepted
7.2.01	1024×1024	413.6880	0.1055	0	Accepted

In addition, this section analyzes the histogram of cipher-images via their variance [39]:

$$VAR(Z) = \frac{1}{N_p} \sum_{i=1}^{N_p} \sum_{j=1}^{N_p} \frac{1}{2} (p_i - p_j)^2 \quad (31)$$

where  $N_p$  represents the gray value, and  $p_i$  and  $p_j$  are the number of pixels whose gray value is  $i$  and  $j$  respectively. When the variance of the histogram is smaller, the pixel distribution is more uniform, and the ability to withstand the statistical attacks is greater.

Table 2 tabulates the variance value of the cipher-image obtained by 2D-CHSLM-IES. It can be observed that the variance values are less than  $5500$ , indicating that the average fluctuation of number of pixels in each gray value is less than  $75$ , which can more effectively withstand the statistical attacks. Table 3 further illustrates the percentage of the variance differences to analyze the effect of changing the key sets on the uniformity of the cipher-image. For  $KS_1$ , the average variance fluctuation is  $0.24\%$ . A tiny modification on  $KS_1$  will obtain the biggest variance fluctuating value  $0.87\%$ , while the smallest one is  $0.001\%$  by changing  $KS_4$ . Those results demonstrate that 2D-CHSLM-IES can withstand the statistical attacks.

**Table 2.** The variance values for different key sets.

Test image	$KS_0$	$KS_1$	$KS_2$	$KS_3$	$KS_4$
5.1.09	5441.8550	5485.7893	5485.2374	5448.9941	5432.9961
5.1.10	5447.6739	5493.1078	5457.2804	5456.3162	5447.6196
5.1.11	5496.4997	5449.3551	5460.8342	5472.1545	5493.2718
5.1.12	5458.7555	5453.2077	5466.7498	5480.9086	5460.4149
5.1.14	5459.1291	5442.7278	5477.9664	5457.8505	5459.0039
5.2.08	5459.5898	5459.0095	5457.9681	5454.6884	5459.5509
5.2.09	5452.3726	5449.8282	5466.6573	5458.529	5452.3228
5.2.10	5472.2117	5468.2702	5463.4145	5432.299	5472.0094
7.1.01	5474.1376	5460.8777	5475.4914	5462.9336	5474.935
7.1.02	5467.3954	5474.5296	5476.7792	5470.1655	5467.7073
7.1.03	5453.6022	5451.4377	5454.1955	5449.8652	5452.765
7.1.04	5474.5494	5459.1821	5446.8977	5456.0021	5472.9866
7.1.05	5462.1370	5446.5362	5460.1792	5460.415	5461.4496
7.1.06	5467.9458	5457.9691	5455.3284	5451.521	5467.192
7.1.07	5474.8764	5455.9308	5465.7357	5466.7098	5474.9154
7.1.08	5446.7922	5467.8586	5455.8798	5462.2921	5447.1123
7.1.09	5455.3019	5456.5913	5470.0106	5465.4739	5454.0027
7.1.10	5467.5594	5479.9682	5477.0743	5451.5287	5468.2064
boat.512	5453.1570	5456.1997	5462.1926	5469.9872	5451.3742

gray21.512	5448.9852	5448.5082	5455.3162	5459.1326	5448.9232
5.3.01	5463.5445	5461.2454	5461.4147	5458.3164	5463.4359
5.3.02	5469.0697	5462.018	5467.0965	5456.1629	5469.5559
7.2.01	5459.3065	5459.6969	5458.9651	5464.6389	5459.9138

Table 3. Percentage of variances difference.

Test image	$KS_1$	$KS_2$	$KS_3$	$KS_4$
5.1.09	0.8	0.79	0.13	0.16
5.1.10	0.83	0.18	0.16	0.001
5.1.11	0.87	0.65	0.44	0.06
5.1.12	0.1	0.15	0.4	0.03
5.1.14	0.3	0.34	0.02	0.002
5.2.08	0.01	0.03	0.09	0.001
5.2.09	0.05	0.26	0.11	0.001
5.2.10	0.07	0.16	0.73	0.004
7.1.01	0.24	0.02	0.21	0.01
7.1.02	0.13	0.17	0.05	0.01
7.1.03	0.04	0.01	0.07	0.02
7.1.04	0.28	0.51	0.34	0.03
7.1.05	0.29	0.04	0.03	0.01
7.1.06	0.18	0.23	0.3	0.01
7.1.07	0.35	0.17	0.15	0.001
7.1.08	0.39	0.17	0.28	0.01
7.1.09	0.02	0.27	0.19	0.02
7.1.10	0.23	0.17	0.29	0.01
boat.512	0.06	0.17	0.31	0.03
gray21.512	0.01	0.12	0.19	0.001
5.3.01	0.04	0.04	0.1	0.002
5.3.02	0.13	0.04	0.24	0.01
7.2.01	0.01	0.01	0.1	0.01
Mean	0.24	0.20	0.21	0.02

5.5. Correlation

It is another statistical analysis method that is used to find the relationship between adjacent pixels of one image, which may be exploited by the attackers. Hence the IES should have the ability of improving the security of the digital image data by breaking the correlation between their neighboring pixels. To test the security of 2D-CHSLM-IES, this section computes the magnitude of the correlation coefficient between neighboring pixels in horizontal (H), vertical (V), and diagonal (D) directions by the randomly 10000-pixel' value of the image via [40]:

$$r_{xy} = \frac{\text{cov}(x,y)}{\sqrt{D(x)}\sqrt{D(y)}} \tag{32}$$

$$\text{cov}(x,y) = \frac{1}{NP} \sum_{i=1}^N (x_i - E(x))(y_i - (E(y))), D(x) = \frac{1}{NP} \sum_{i=1}^N (x_i - E(x))^2, E(x) = \frac{1}{NP} \sum_{i=1}^N x_i \tag{33}$$

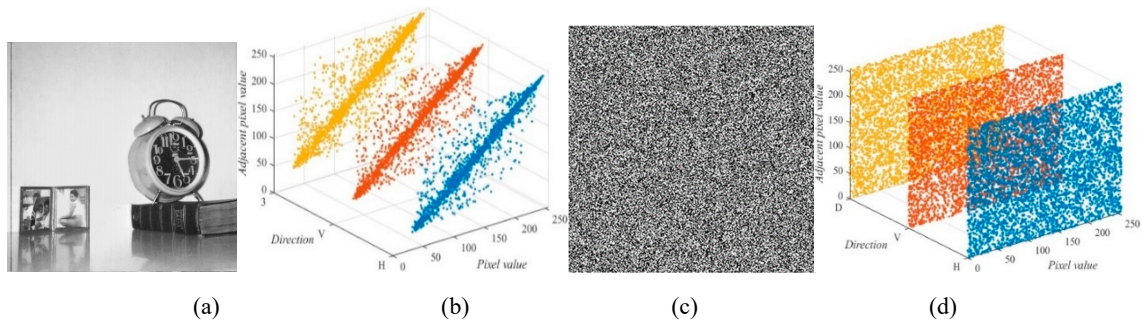
where  $x$  and  $y$  represent pixel values of two neighboring pixels,  $NP$  is the chosen number of pixels.  $\text{cov}(x, y)$  is the covariance of  $x$  and  $y$ .  $D(x)$  and  $E(x)$  is the variance and expectation, respectively. When  $r_{xy}$  close to 1, it means a high correlation, otherwise, a low correlation.

Table 4 illustrates the correlation coefficient results of the different plain-images and the corresponding cipher-images for all three directions. As can be observed in Table 4, the correlation between the pixel value is high in the case of plain-images whereas the correlation of the cipher-image is near 0. Moreover, Table 4 compares the correlation coefficient results with Ref. [41]. Obviously, 2D-CHSLM-IES has a lower correlation than those IESs in all three directions. It implies that 2D-CHSLM-IES is highly resist the statistical attacks.

**Table 4.** Correlations of two adjacent pixels on three directions and their comparison results.

Test image	2D-CHSLM-IES						Ref. [41]		
	Plain-image			Cipher-image			Cipher-image		
	H	V	D	H	V	D	H	V	D
5.1.09	0.9094	0.9053	0.8989	0.003	-0.0029	-0.0017	0.0162	-0.0139	0.0025
5.1.10	0.8242	0.8047	0.7928	0.0012	-0.0034	0.0016	-0.0258	0.0041	0.0009
5.1.11	0.8898	0.8512	0.9212	0.001	0.0029	0.0019	-0.0016	-0.0012	0.0141
5.1.12	0.9485	0.9498	0.9308	0.0031	-0.0033	-0.0018	-0.0114	-0.0097	0.0034
5.1.13	0.7512	0.7549	0.7874	0.0042	0.0048	0.0015	0.0070	0.0100	-0.0097
5.1.14	0.8583	0.8597	0.856	-0.0012	0.0011	-0.004	-0.0176	-0.0054	-0.0196
5.2.08	0.8387	0.8374	0.8813	-0.0012	-0.0032	-0.002	-0.0028	0.0046	0.0124
5.2.09	0.7839	0.8213	0.817	-0.001	-0.0016	0.0031	-0.0172	-0.0091	-0.0178
5.2.10	0.8824	0.9038	0.901	-0.0028	-0.0011	0.0036	-0.0190	0.0005	-0.0050
7.1.01	0.8975	0.9038	0.9128	-0.0024	-0.0024	0.0023	0.0195	-0.0070	-0.0165
7.1.02	0.9038	0.897	0.8766	-0.0025	0.0026	-0.0047	0.0291	-0.0176	-0.0080
7.1.03	0.8924	0.8931	0.8983	-0.0016	0.003	-0.0019	-0.0293	-0.0091	0.0086
7.1.04	0.9607	0.9529	0.9543	0.0015	-0.0022	-0.0018	-0.0005	0.0026	0.0030
7.1.05	0.8827	0.8932	0.8949	-0.0013	0.0032	-0.0007	-0.0126	0.0044	0.0004
7.1.06	0.8787	0.8772	0.8743	0.0037	0.0017	-0.003	0.0161	0.0110	0.0032
7.1.07	0.8436	0.8454	0.8444	-0.0001	-0.0029	-0.0028	0.0017	-0.0194	-0.0076
7.1.08	0.9208	0.9114	0.9276	0.0023	-0.0041	-0.0035	0.0006	-0.0142	0.00002
7.1.09	0.9187	0.9135	0.9073	0.0039	-0.0029	-0.0036	-0.0047	0.0149	0.0089
7.1.10	0.9192	0.9423	0.9437	0.0047	0.0048	0.0035	0.0051	-0.0109	0.0144
boat.512	0.9257	0.9405	0.9276	0.0035	0.0008	-0.0048	-0.0045	-0.0011	-0.0113
gray21.512	0.999	0.994	0.9974	0.0011	0.0012	0.0042	-0.0086	-0.0145	0.0068
ruler.512	0.0425	-0.0708	-0.0811	-0.0014	0.0025	-0.0025	-0.0035	-0.0085	0.0165
5.3.01	0.9665	0.9625	0.9694	-0.0022	0.0035	-0.0037	-0.0057	-0.0069	0.0040
5.3.02	0.8712	0.8444	0.8557	0.0027	-0.0004	-0.0035	-0.0137	0.0007	0.0091
7.2.01	0.9398	0.9562	0.9486	0.0024	0.0012	0.0026	-0.0032	0.0032	0.0047

Figure 16 depicts the correlation coefficient of the plain-image “5.1.12” and their corresponding cipher-image. As can be seen, the correlation coefficient results are scattered around a straight line which indicates a high correlation for all three directions. On the contrary, the correlation coefficient results of the cipher-image are scattered evenly on the plane which indicates that the image information has extremely low relationships among them after 2D-CHSLM-IES operations.



**Figure 16.** Correlation analysis: (a) the plain-image “5.1.12” and (b) the adjacent pixel correlation on three directions; the cipher-image of Figure 16(a) and (d) the adjacent pixel correlation on three directions.

5.6. Information entropy

Information entropy is another metric of the statistical analysis. It is used to quantitatively analyze the randomness of the image data. The higher the information entropy, the higher the usable data, a good IES should process the image with an information entropy near 0. The entropy can be calculated via:

$$H(x) = - \sum_{i=1}^L P(x_i) \log_2 P(x_i) \tag{34}$$

where  $L$  is the number of gray levels present in an image, while  $P(x_i)$  is the probability of a specific gray level  $x_i$  occurring in the image. For a grayscale image ( $L = 255$ ), their ideal value of  $H$  is 8. Thus, the cipher-image with a  $H$  near 8 means greater randomness and better effect. Table 5 tabulates the computed  $H$  of different plaint-images and the cipher-images using 2D-CHSLM-IES. Moreover, Table 5 also compare the computed  $H$  with other IESs [41–43]. The results imply that 2D-CHSLM-IES performs tremendous encryption performance.

**Table 5.** Information entropy results of 2D-CHSLM-IES and their comparison results.

Test image	Plain-image	Cipher-image			
		Ref. [41]	Ref. [42]	Ref. [43]	2D-CHSLM-IES
5.1.09	6.7057	7.996950	7.9973	7.9972	7.9972
5.1.10	1.5483	7.997474	7.9973	7.9977	7.9975
5.1.11	7.3424	7.997126	7.9968	7.9971	7.9976
5.1.12	7.2010	7.997025	7.9975	7.9972	7.9973
5.1.13	6.9940	7.996947	7.9975	7.9970	7.9972
5.1.14	5.7056	7.997028	7.9973	7.9970	7.9973
5.2.08	6.0274	7.999341	7.9993	7.9993	7.9993
5.2.09	4.0045	7.999300	7.9992	7.9991	7.9993
5.2.10	5.4957	7.999381	7.9993	7.9991	7.9992
7.1.01	6.1074	7.999235	7.9993	7.9993	7.9993
7.1.02	6.5632	7.999330	7.9993	7.9994	7.9991
7.1.03	6.6953	7.999262	7.9993	7.9993	7.9993
7.1.04	5.9916	7.999299	7.9993	7.9994	7.9994
7.1.05	5.0534	7.999333	7.9994	7.9992	7.9992
7.1.06	6.1898	7.999267	7.9992	7.9993	7.9993
7.1.07	5.9088	7.999211	7.9994	7.9993	7.9991
7.1.08	7.1914	7.999171	-	7.9993	7.9994
7.1.09	4.3923	7.999268	-	7.9993	7.9992
7.1.10	0.5000	7.999337	-	7.9992	7.9994
boat.512	7.5237	7.999179	7.9993	7.9993	7.9993

gray21.512	6.8303	7.999454	7.9993	7.9994	7.9993
ruler.512	5.6415	7.999270	7.9993	7.9992	7.9991
5.3.01	6.7057	7.999829	7.9998	7.9998	7.9998
5.3.02	1.5483	7.999851	7.9998	7.9998	7.9998
7.2.01	7.3424	7.999821	7.9998	7.9998	7.9997
Mean of 256×256	6.0116	7.997091	7.9973	7.9972	7.9974
Mean of 512×512	5.6263	7.999290	7.9993	7.9993	7.9993
Mean of 1024×1024	6.6652	7.999834	7.9998	7.9998	7.9998

### 5.7. Differential attack

Similar to Section 5.3, the differential attack is a way to analyze the sensitivity of one IES. In this attack, the hacker tries to find the statistical patterns of an image. There are two commonly metrics to measure the ability of an IES against the differential attacks, Number of Pixels Change Rate ( *NPCR* ) and Unified Average Changing Intensity ( *UACI* ). The numerical equations are as follows:

$$NPCR = \frac{\sum_{i=1}^M \sum_{j=1}^N D(i, j)}{M \times N} \times 100\% \quad (35)$$

$$D(i, j) = \begin{cases} 1 & \text{if } c_1(i, j) \neq c_2(i, j) \\ 0 & \text{if } c_1(i, j) = c_2(i, j) \end{cases}$$

$$UACI = \frac{1}{M \times N} \left( \sum_{i=1}^M \sum_{j=1}^N \frac{|c_1(i, j) - c_2(i, j)|}{255} \right) \times 100\% \quad (36)$$

Among Eq. (35) and Eq. (36),  $M$  and  $N$  are the rows and columns of an image, respectively.  $c_1$  and  $c_2$  represent two cipher-images which their original images have only one pixel value that is slightly different. The theoretical values are  $255 / 256 \times 100\% \approx 99.60938\%$  and  $257 / 768 \times 100\% \approx 33.46354\%$ , respectively.

Moreover, the acceptable intervals for *NPCR* and *UACI* are given in the REF at the significance  $\alpha$  [44]:

$$NPCR > \frac{L - \Phi^{-1}(\alpha) \sqrt{\frac{L}{M \times N}}}{L + 1} \quad (37)$$

$$\frac{L + 2}{3 \times L + 3} - \Phi^{-1}\left(\frac{\alpha}{2}\right) \sqrt{\frac{(L + 2) \times (L^2 + 2 \times L + 3)}{18 \times (L + 1)^2 \times L \times M \times N}} \leq UACI \leq \frac{L + 2}{3 \times L + 3} + \Phi^{-1}\left(\frac{\alpha}{2}\right) \sqrt{\frac{(L + 2) \times (L^2 + 2 \times L + 3)}{18 \times (L + 1)^2 \times L \times M \times N}} \quad (38)$$

where  $L = 255$  when  $\alpha = 0.05$ ,  $\Phi^{-1}(\alpha) = 1.645$ , and  $\Phi^{-1}(\frac{\alpha}{2}) = 1.96$ . Table 6 tabulates the ranges of *NPCR* and *UACI* for images of different sizes.

**Table 6.** Ranges of *NPCR* and *UACI* ( $\alpha = 0.05$ ).

<i>NPCR</i> , <i>UACI</i>	Critical values (%) ( $M, N$ )		
	$(M, N) = (256, 256)$	$(M, N) = (512, 512)$	$(M, N) = (1024, 1024)$
$NPCR_{\alpha}^*$	99.5693	99.5893	99.5994
$UACI_{\alpha}^{*+}$	33.2824	33.3730	33.4182
$UACI_{\alpha}^{*-}$	33.6447	33.5541	33.5088

Table 7 tabulates the obtained *NPCR* and *UACI* scores for different images and compare them with other IESs. Obviously, all scores are totally near their theoretical scores than all other

methods. Also, the obtained scores of *NPCR* and *UACI* have been analyzed for significance value at  $\alpha = 0.05$  [44]. It is not hard to find that 2D-CHSLM-IES passes the tests, which indicates the ability of 2D-CHSLM-IES against the differential attacks.

Table 7. *NPCR*(%) and *UACI*(%) evaluation.

Test image	<i>NPCR</i> (%)				<i>UACI</i> (%)			
	Ref. [41]	Ref. [42]	Ref. [43]	2D-CHSLM-IES	Ref. [41]	Ref. [42]	Ref. [43]	2D-CHSLM-IES
256×256: $NPCR_{\alpha}^{*} \geq 99.5693$					256×256: $(UACI_{\alpha}^{*+}, UACI_{\alpha}^{*-}) = (33.2824, 33.6447)$			
5.1.09	99.6002	99.6323	99.6094	99.6109	33.4831	33.4561	33.4817	33.4330
5.1.10	99.6170	99.6124	99.6185	99.6140	33.5384	33.5674	33.4672	33.4606
5.1.11	99.6292	99.6078	99.6048	99.6185	33.5100	33.4934	33.4216	33.4543
5.1.12	99.6109	99.6185	99.6094	99.6231	33.3905	33.4669	33.4362	33.5017
5.1.13	99.6307	99.5956	99.6109	99.6124	33.4601	33.4151	33.4393	33.4913
5.1.14	99.5911	99.6292	99.6002	99.6353	33.4052	33.4585	33.4646	33.4260
512×512: $NPCR_{\alpha}^{*} \geq 99.5893$					512×512: $(UACI_{\alpha}^{*+}, UACI_{\alpha}^{*-}) = (33.3730, 33.5541)$			
5.2.08	99.5972	99.6193	99.6109	99.6265	33.4380	33.4772	33.4865	33.4330
5.2.09	99.6265	99.6178	99.6090	99.6098	33.5115	33.4369	33.4788	33.4977
5.2.10	99.6216	99.6323	99.6086	99.6059	33.5257	33.4081	33.5094	33.4794
7.1.01	99.6098	99.6204	99.6071	99.6040	33.4190	33.4324	33.4632	33.4694
7.1.02	99.6189	99.6101	99.6094	99.6212	33.5257	33.4435	33.4572	33.4410
7.1.03	99.6273	99.5975	99.6098	99.6151	33.5024	33.4653	33.4241	33.4801
7.1.04	99.5979	99.6113	99.6117	99.6014	33.4243	33.4360	33.4671	33.4845
7.1.05	99.6120	99.6159	99.6105	99.6109	33.4230	33.4468	33.4469	33.4939
7.1.06	99.6056	99.6162	99.6117	99.6124	33.4550	33.4857	33.4557	33.4338
7.1.07	99.6029	99.6086	99.6101	99.6170	33.4514	33.4385	33.4847	33.4455
7.1.08	99.5998	-	99.6162	99.6105	33.4468	-	33.4796	33.4877
7.1.09	99.6220	-	99.6071	99.6334	33.4605	-	33.4256	33.4918
7.1.10	99.6254	-	99.6109	99.6044	33.4698	-	33.4636	33.5007
boat.512	99.6120	99.6078	99.6033	99.6151	33.4356	33.4853	33.4305	33.4436
gray21.512	99.6025	99.6227	99.6094	99.6216	33.4369	33.4007	33.4916	33.4577
ruler.512	99.5983	99.6216	99.6098	99.6033	33.4237	33.4343	33.5110	33.4847
1024×1024: $NPCR_{\alpha}^{*} \geq 99.5994$					1024×1024: $(UACI_{\alpha}^{*+}, UACI_{\alpha}^{*-}) = (33.4182, 33.5088)$			
5.3.01	99.6127	99.6024	99.6094	99.61	33.4455	33.4902	33.4775	33.4914
5.3.02	99.6151	99.6009	99.6076	99.6081	33.4942	33.4440	33.4646	33.4433
7.2.01	99.6058	99.6059	99.6033	99.6043	33.4597	33.4598	33.4697	33.4309
Pass/All	25/25	22/22	25/25	25/25	25/25	22/22	25/25	25/25
Mean	99.611696	99.6139	99.6092	99.6140	33.461440	33.4565	33.4639	33.4663

5.8. Noise and data loss attacks

Robustness is a significant metric to measure the anti-interference ability of an IES. This section verifies the robustness of 2D-CHSLM-IES against the two common corruption sources, noise attack and data loss attack respectively.

#### 5.8.1. Robust to noise attacks

Noise attack is a common corruption source during transmission. An effective IES must be robust to this kind types of attacks. The main noises include speckle noise, pepper and salt noise, etc. This section analyzes the effect of adding those two noises to the cipher-image “gray21.512”. On the premise that the key set remains unchanged, different intensities of the pepper and salt noise are added to the cipher-image. Then 2D-CHSLM-IDS is used to decode these cipher-images. Figure 17 depicts the cipher-images with different noise intensities (0.01, 0.05, 0.0001, and 0.0005) and their corresponding decoded images by 2D-CHSLM-IDS. As shown in Figure 17, even if the noise intensity reaches 0.05 and 0.0005, we can still recognize their original image. Hence 2D-CHSLM-IES is effective to the noise attacks.

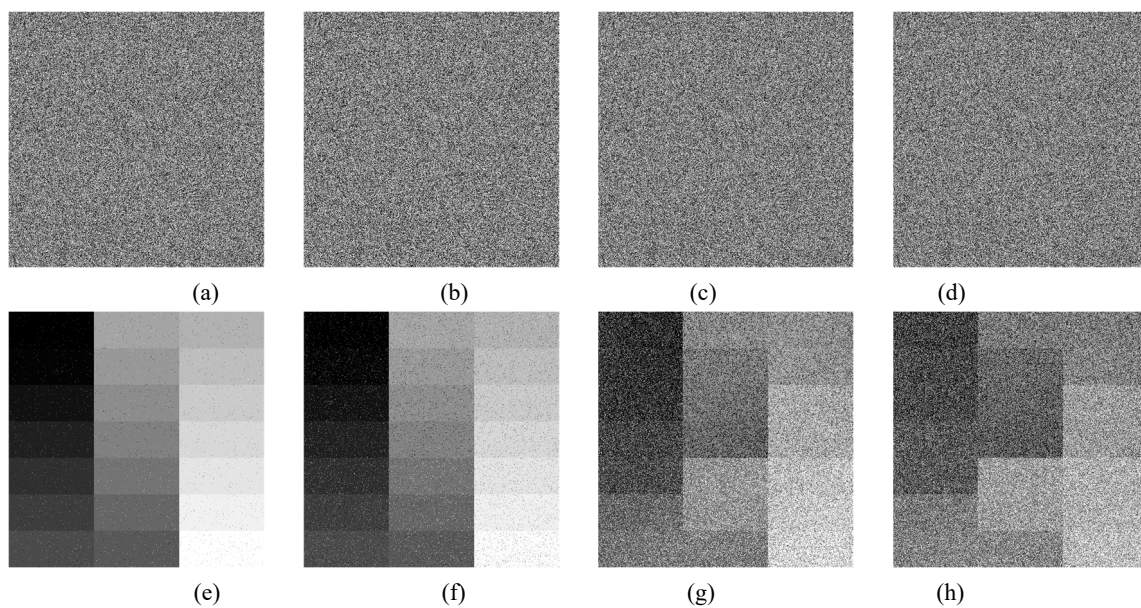


**Figure 17.** Noise attacks: the cipher-image “gray21.512” with the salt-and-pepper noise intensity of (a) 0.01 and (b) 0.05, and the speckle noise intensity of (c) 0.0001 and (d) 0.0005, Figures. 17(e-h) are the cipher-image of Figures. 17(a-d).

#### 5.8.2. Robust to data loss attacks

Data loss attack is another common corruption source during transmission. An effective IES must be robust to this kind types of attacks. The usual approach is to assume that the cipher-image has lost different proportions of data, and then use IES to try to decode their corresponding original image. Obviously, as the proportion of data loss increases, the quality of the decrypted image gradually decreases. Figure 18 depicts the cipher-images “5.3.01” with different proportions ( $1/64$ ,  $1/8$ , and  $1/2$ ) of data loss and their corresponding decoded images. As shown in Figure 18, the main information can still recognize from their decoded image. Hence 2D-CHSLM-IES is effective to the data loss attacks. It means that 2D-CHSLM-IES is robust to noise and data loss attacks.

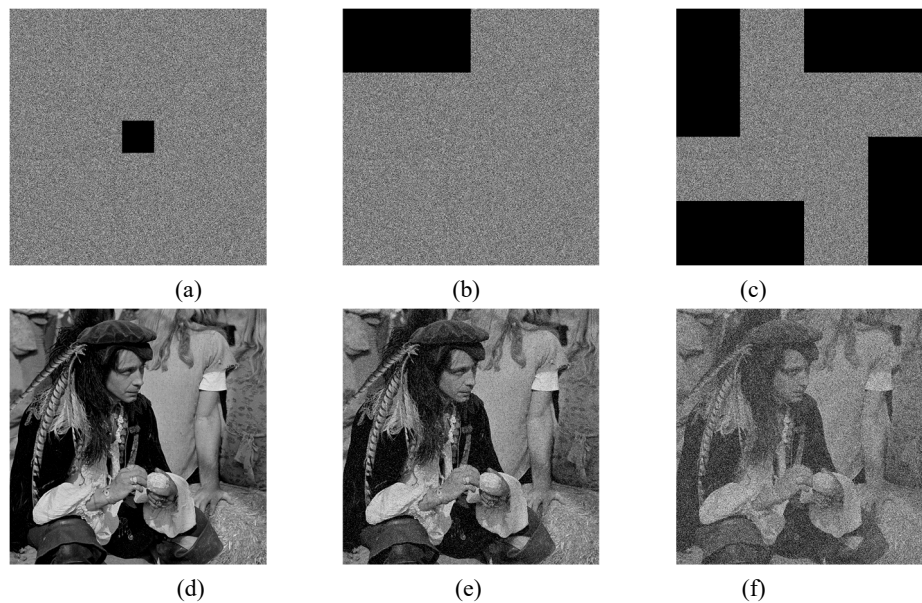


**Figure 18.** Data loss attacks: the cipher-image “5.3.1” lose data with (a)  $1/64$ , (b)  $1/8$  and (c)  $1/2$ , respectively; and the decoded image of (d) Figure 18(a), (e) Figure 18(b), and (h) Figure 18(c).

## 6. Conclusion

In this paper, a new bit-level IES based on 2D-CHSLM is designed, which uses Zig-zag transforms and cross coupled diffusion strategy to enhance security. 2D-CHSLM performs complex hyperchaotic characteristics and is highly suitable for application in IES, which are verified by their BD and trajectory diagrams, LE, SE, COs and PE, and 0-1 test respectively. The chaotic sequence generated by 2D-CHSLM is used to encrypt the plain-image, which largely improves the key sensitivity of 2D-CHSLM-IES. 2D-CHSLM-based bit-level confusion using Zig-zag transform and 2D-CHSLM-based cross coupled diffusion strategy can further enhance the security level. The proposed 2D-CHSLM-IES is robust to the common types of attacks, such as the brute force attacks, statistical attacks, differential attacks, noise and data loss attacks, and its comprehensive performance is superior than other advanced IESs.

**Acknowledgements:** This work is supported by the National Natural Science Foundation of China (Nos: 62176037 and 61701070), the Fundamental Research Funds for the Central Universities (Nos:3132023252), China Postdoctoral Science Foundation (No: 2020M680933).

## References

1. Liu H, Liu J, Ma C. Constructing dynamic strong S-Box using 3D chaotic map and application to image encryption. *Multimed Tools Appl.*, 2023, 82(16): 23899-23914.
2. Xia Z, Wang X, Zhou W, Li R, Wang C, Zhang C. Color medical image lossless watermarking using chaotic system and accurate quaternion polar harmonic transforms. *Signal Process.*, 2019, 157: 108-118.
3. Wei Z. Dynamical behaviors of a chaotic system with no equilibria. *Phys Lett A*, 2011, 376(2):102-108.
4. Peng H-H, Xu X-M, Yang B-C, Yin L-Z. Implication of two-coupled differential Van der Pol duffing oscillator in weak signal detection. *J Phys Soc Jpn*, 2016, 85(4): 044005.
5. Boriga R, Dascalescu AC, Priescu I. A new hyperchaotic map and its application in an image encryption scheme. *Signal Process: Image Commun* 2014;29:887-901.
6. Wang M, Wang X, Wang C, Zhou S, Xia Z, Li Q. Color image encryption based on 2D enhanced hyperchaotic logistic-sine map and two-way Josephus traversing. *Digit. Signal Process.*, 2023, 132:103818.
7. Alsubaei F S, Alneil A A, Mohamed A, Hilal A M. Block-Scrambling-Based Encryption with Deep-Learning-Driven Remote Sensing Image Classification. *Remote Sens*, 2023, 15(4): 1022.
8. Hu Y, Nan L. Image encryption algorithm based on 1D-SFACF with cross-cyclic shift and adaptive diffusion. *Phys Scr.*, 2023, 98(5): 055209.

9. Yan X, Wang X, Xian Y. Chaotic image encryption algorithm based on arithmetic sequence scrambling model and DNA encoding operation. *Multimed Tools Appl.*, 2022, 80(7): 10949-10983.
10. Wang M, Wang X, Wang C, Xia Z, Zhou S. Novel Image Compression-Then-Encryption Scheme Based on 2D Cross Coupled Map Lattice and Compressive Sensing. *Multimed Tools Appl.*, 2023, Doi: 10.1007/s11042-023-15286-0.
11. Wu Y, Yang G, Jin H, Noonan J P. Image encryption using the two-dimensional logistic chaotic map. *J Electron Imaging.*, 2012, 21(1): 013014.
12. Hua Z, Zhou Y, Pun CM, Chen C. 2D Sine Logistic modulation map for image encryption. *Inf Sci.*, 2014, 297: 80-94.
13. Sharma M. Image encryption based on a new 2D logistic adjusted logistic map. *Multimed. Tools Appl.*, 2020, 79(1-2): 355-374.
14. Zhu H, Zhao Y, Song Y. 2D Logistic-Modulated-Sine-Coupling-Logistic Chaotic Map for Image Encryption. *IEEE Access*, 2019, 7:14081-14098.
15. Teng L, Wang X, Xian, Y. Image encryption algorithm based on 2D-CLSS hyperchaotic map using simultaneous permutation and diffusion. *Inf Sci.*, 2022, 605: 71-85.
16. Matthews R. On the derivation of a chaotic encryption algorithm. *Cryptologia*, 1989, 13(1): 29-42.
17. Wang M, Wang X, Zhao T, Zhang C, Xia Z, Yao N. Spatiotemporal chaos in improved Cross Coupled Map Lattice and its application in a bit-level image encryption scheme. *Inf Sci.*, 2021, 544: 1-24.
18. Zhang Z, Tang J, Ni H, Huang T. Image adaptive encryption algorithm using a novel 2D chaotic system. *Nonlinear Dyn.*, 2023, 111(11): 10629-10652.
19. Zhou S, Zhao Z, Wang X. Novel chaotic colour image cryptosystem with deep learning. *Chaos Soliton Fract.*, 2022, 161: 112380.
20. Lai Q, Liu Y. A cross-channel color image encryption algorithm using two-dimensional hyperchaotic map. *Expert Syst Appl.*, 2023, 223: 119923.
21. Peng F, Zhang X, Lin Z, Long M. A tunable selective encryption scheme for H.265/HEVC based on chroma IPM and coefficient scrambling. *IEEE Trans Circuits Syst Video Technol*, 2020, 30(8): 2765-2780.
22. Wu Y, Zhou Y, Saveriades G, Agaian S, Noonan J P, Natarajan P. Local Shannon entropy measure with statistical tests for image randomness. *Inf Sci.*, 2022, 222:323-342.
23. Tang Z, Song J, Zhang X, Sun R. Multiple-image encryption with bit-plane decomposition and chaotic maps. *Opt Lasers Eng.*, 2016, 80: 1-11.
24. Wang M, Wang X, Wang C, Xia Z, Zhao H, Gao S, Zhou S, Yao N. Spatiotemporal chaos in cross coupled map lattice with dynamic coupling coefficient and its application in bit-level color image encryption. *Chaos Soliton Fract.*, 2020, 139: 110028.
25. Wang M, Liu H, Zhao M. Bit-level image encryption algorithm based on random-time S-Box substitution. *Eur. Phys. J. Spec. Top.*, 2022, 231(16-17): 3225-3237.
26. Li J, Wang J, Di X. Image encryption algorithm based on bit-level permutation and "Feistel-like network" diffusion. *Multimed Tools Appl.*, 2022, 81(30): 44335-44362.
27. Devipriya M, Brindha M. Image encryption using modified perfect shuffle-based bit level permutation and learning with errors based diffusion for IoT. *Comput Electr Eng*, 2022, 100:107954.
28. Luo J, Xu X, Ding Y, Yuan Y, Yang B, Sun K, Yin L. Application of a memristor-based oscillator to weak signal detection. *Eur. Phys. J. Plus*, 2018, 133(6): 239.
29. ul Haq T, Shah T. 4D mixed chaotic system and its application to RGB image encryption using substitution diffusion. *J Inf Secur Appl*, 2021, 61: 102931.
30. Wang X, Guan N. 2D sine-logistic-tent-coupling map for image encryption. *J. Ambient. Intell. Humaniz. Comput*, 2022, 1-21.
31. Wang X, Guan N, Yang J. Image encryption algorithm with random scrambling based on one-dimensional logistic self-embedding chaotic map. *Chaos Soliton Fract.*, 2021, 150: 111117.
32. Li Y, Li C, Liu S, Hua Z, Jiang H. A 2-D conditional symmetric hyperchaotic map with complete control. *Nonlinear Dyn.*, 2022, 109(2): 1155-1165.
33. Hu X, Jiang D, Ahmad M, Tsafack N, Zhu L, Zheng M. Novel 3-D hyperchaotic map with hidden attractor and its application in meaningful image encryption. *Nonlinear Dyn.*, 2023, 111(20): 19487-19512.
34. Richman J, Moorman J. Physiological time-series analysis using approximate entropy and sample entropy. *American Journal of Physiology-Heart and Circulatory Physiology*, 2000, 278(6): H2039-H2049.
35. Gao X. Image encryption algorithm based on 2D hyperchaotic map. *Opt. Laser Technol.*, 2021, 142: 107252.

36. Huo D, Zhu Z, Wei L, Han C, Zhou X. A visually secure image encryption scheme based on compressive sensing. *Opt. Commun.*, 2021, 492: 126976.
37. Mao N, Tong X, Zhang M, Wang Z. Real-time image encryption algorithm based on combined chaotic map and optimized lifting wavelet transform. *J Real-Time Image Pr.*, 2023, 20(2): 35.
38. C. Cao, K. Sun, W. Liu. A novel bit-level image encryption algorithm based on 2D-LICM hyperchaotic map. *Signal Process.*, 2018, 143: 122-133.
39. Parida P, Pradhan, Pradhan C, Gao X, Roy D S, Barik R K. Image encryption and authentication with elliptic curve cryptography and multidimensional chaotic maps. *IEEE Access*, 2021, 9: 76191-76204.
40. Wang M, Wang X, Zhang Y, Zhou S, Zhao T, Yao N. A novel chaotic system and its application in a color image cryptosystem. *Opt Lasers Eng.*, 2019, 121: 479-494.
41. Wang X, Chen X, Zhao M. A new two-dimensional sine-coupled-logistic map and its application in image encryption. *Multimed Tools Appl.*, 2023, 82(23): 35719-35755.
42. Wang X, Zhao M. A new spatiotemporal chaos model and its application in bit-level image encryption. *Multimed Tools Appl.*, 2023, Doi: 10.1007/s11042-023-16031-3.
43. Liang Q, Zhu C. A new one-dimensional chaotic map for image encryption scheme based on random DNA coding. *Opt. Laser Technol.*, 2023, 160:109033.
44. Wu Y, Noonan J P, Agaian S. NPCR and UACI randomness tests for image encryption. *Cyber J., Multidiscipl. J. Sci. Technol., J. Sel. Areas Telecommun.* 2011, 1(2): 31-38.

**Disclaimer/Publisher's Note:** The statements, opinions and data contained in all publications are solely those of the individual author(s) and contributor(s) and not of MDPI and/or the editor(s). MDPI and/or the editor(s) disclaim responsibility for any injury to people or property resulting from any ideas, methods, instructions or products referred to in the content.